NIST Technical Note 1881

Self Training of a Fault-Free Model for Residential Air Conditioner Fault Detection and Diagnostics

Jaehyeok Heo
W. Vance Payne
Piotr A. Domanski
Zhimin Du

http://dx.doi.org/10.6028/NIST.TN.1881

National Institute of Standards and Technology
U.S. Department of Commerce

NIST Technical Note 1881

Self Training of a Fault-Free Model for Residential Air Conditioner Fault Detection and Diagnostics

Jaehyeok Heo
Korea Institute of Energy Research
New and Renewable Energy Research Division
Solar Thermal Laboratory

W. Vance Payne
Piotr A. Domanski
National Institute of Standards and Technology
Energy and Environment Division
Engineering Laboratory

Zhimin Du
School of Mechanical Engineering
Shanghai Jiao tong University

http://dx.doi.org/10.6028/NIST.TN.1881

May 2015

U.S. Department of Commerce
Penny Pritzker, Secretary

National Institute of Standards and Technology
Willie May, Under Secretary of Commerce for Standards and Technology and Director

Use of Non-SI Units in a NIST Publication

The policy of the National Institute of Standards and Technology is to use the International System of Units (metric units) in all of its publications. However, in North America in the heating, ventilation and air-conditioning industry, certain non-SI units are so widely used instead of SI units that it is more practical and less confusing to include some measurement values in customary units only.

National Institute of Standards and Technology Technical Note 1881
Natl. Inst. Stand. Technol. Tech. Note 1881, 44 pages (May 2015)
http://dx.doi.org/10.6028/NIST.TN.1881
CODEN: NTNOEF

Contents

Nomenclature

Symbols

a	coefficient of multivariable polynomial or a constant
C	case variable
d	data distance to zone center
d_{max}	maximum distance of the filtered group in the zone
h	variables of the hidden layer neurons
m	number of coefficients, number of features to determine fault pattern
N	number of data, normal distribution
O	variable of output neuron
P	pressure (kPa) or probability
r	residual
s	positive constant multiplier of the threshold
T	temperature (^{o}F)
w	weight matrix
W	work (W)
x	variable representing measured data
X	variables of the input layer neurons, independent variables
z	standardized feature residual

Greek Symbols

α	learning rate
δ	an error information term
Δ	difference
ε	threshold value
μ	momentum terms, predicted value by fault-free models
σ	standard deviation
ϕ	feature parameter

Subscripts

C	condenser
CA	condenser air
D	compressor discharge
DB	dry bulb
DP	dew point
E	evaporator
EA	evaporator air
FF	fault free
ID	indoor
IDP	indoor dew point
OD	outdoor
sat	saturation

SC	subcooling
SH	superheat

Abbreviations

AC	air conditioner
ANN	artificial neural network
avg	average
CF	condenser fouling, reduced outdoor air flow rate
CMF	compressor valve leakage
COP	coefficient of performance
DCR	domain coverage rate
EF	evaporator fouling, improper indoor air flow rate
erf	error function
FDD	fault detection and diagnosis
FF	fault free
HP	heat pump
IoT	Internet of things
LL	liquid line restriction
MPR	multivariable polynomial regression
NC	presence of non-condensable gases
OC	refrigerant overcharge
PDF	probability density function
RH	relative humidity
SDR	successful diagnosis rate (%)
trans	transfer function
TRE	test relative error (%)
TSE	test standard error (^{o}F)
UC	refrigerant undercharge
ZD	zone density

1. Introduction

In 2014, residential cooling consumed 13 % of the total U.S. residential home electrical energy used (189 of 1415 billion kWh) according to the U.S. Energy Information Administration (EIA, 2014). Therefore, efficient maintenance techniques for cooling systems are very important in preventing energy waste due to improper operation and lack of fault recognition. If a fault detection and diagnostic (FDD) system could save 1 % of the 189 billion kWh used for cooling, it would have saved consumers approximately $229 million (EIA, 2013). However, building and applying a generic FDD model is very difficult due to the various installation environments seen for residential air-conditioning and heat pump systems. Self training FDD methods are the only way to implement an effective FDD method in these varied installation environments.

Fault Detection and Diagnostics (FDD) can be used to commission and maintain the performance of residential style, split-system, air conditioners and heat pumps. Previous investigations by various researchers have provided techniques for detecting and diagnosing all common faults, but these techniques are meant to be applied to systems that have been thoroughly tested in a carefully instrumented laboratory environment. Although such an approach can be applied to factory-assembled systems, installation variations of field-assembled systems require in-situ adaptation of FDD methods. Providing a workable solution to this problem has been the impetus for the work presented in this report, which describes a method for adapting laboratory generated FDD techniques to field installed systems by automatically customizing the FDD fault-free performance models to random installation differences.

2. Overview of Fault Detection and Diagnostics

2.1. Previous Studies

The development of this fault detection and diagnostics (FDD) method required both extensive measurements and analytical efforts. System characteristics were measured during fault-free and faulty operation, and analytical work implemented that knowledge and data into algorithms able to produce a robust determination of the 'health' of the system. In earlier work the National Institute of Standards and Technology (NIST) made detailed measurements on the cooling (Kim et al., 2006) and heating [(Payne et al., 2009), (Yoon et al., 2011)] performance of a residential, split-system, air-source, heat pump with faults imposed. Previous research on FDD techniques [e.g.,(Rossi and Braun, 1997), (Braun, 1999), (Chen and Braun, 2001)] was used to refine a rule-based chart technique able to detect and diagnose common faults which can occur during operation of an air conditioner (AC) and heat pump (HP) [(Kim et al., 2008b),(Kim et al., 2010)].

2.2. Concept of Self Training

System parameters sensitive to common faults were identified, such as refrigerant subcooling at the condenser outlet or a difference in the air temperature between the inlet and outlet of the heat exchanger. These parameters are referred to as features. The values of these features during fault-free heat pump operation were correlated and modeled as functions of different operating conditions. After models of the fault-free features have been developed, detection of a fault (if it exists) and its diagnosis can be done by comparing features' fault-free values to those measured during heat pump operation. Typically, fault-free features are measured and correlated for steady-state operation. For this reason, feature measurements during regular heat pump operation must be taken only when the system is steady-state.

For factory-assembled systems, e.g., windows air conditioners or roof-top units, fault-free features can be measured in a laboratory to establish a representation for that model line. These feature measurements (and derived correlations) can be applied to the entire model line of the tested system. However, for field-assembled systems, such as split, air-to-air heat pumps and air conditioners, their fault-free characteristics may substantially differ due to their individual installation constraints. For this reason, for field-assembled systems, fault-free feature models need to be developed based on data collected in-situ after the system has been installed. This challenging task can be carried out by a self training module incorporated into the FDD unit.

The self training module is started by a technician after completing a manual check of the installed system per manufacturer instructions and ensuring the system operates free of faults. During operation the self training module receives measurements of system features and operating conditions, and processes them according to the scheme shown in Figure 2.1.

First, the steady-state detector evaluates the data and determines whether the heat pump operation is steady. In the next step, the data are screened by the fault-free filter. This filter can be considered as a preliminary FDD scheme provided by the outdoor unit manufacturer. It contains preliminary models for predicting fault-free values of system features and uses relaxed thresholds to accommodate different installation constraints and their impact on the system features. The purpose of this screening is to identify significant departures of the measured features from preliminary fault-free values and signal them as possible installation errors. In such an instance, the self training process would be halted and could only be re-initiated by manual restart.

Filtered data from a steady-state detector are recorded until the data are considered fault-free based upon quality and distribution within the selected range of specific operating conditions (independent variables): outdoor dry-bulb, indoor dry-bulb, and indoor humidity. The Zone Density test considers the current independent variables and determines if they are better than

any other previously collected data within some predefined variation. If the data are acceptable, a decision is made to produce an intermediate fault-free correlation for all of the dependent features. These intermediate fault-free correlations are used as new fault-free tests to select more fault-free data. The self training process consists of generating several intermediate fault-free models, with a new model replacing an older one as additional fault-free data are collected, expanding the self training dataset used to develop the previous model. If a new intermediate set of correlations is developed, then the extents of the independent variables are examined to determine whether the desired range has been covered. This data collection process continues, and the models are updated until the operating conditions domain coverage (or preselected extents of the independent variables) reaches a maximum value. Once the domain coverage is at the maximum value the final fault-free correlations are generated and self training is complete. The concepts of Zone Density and Coverage Rate will be discussed further in the following sections.

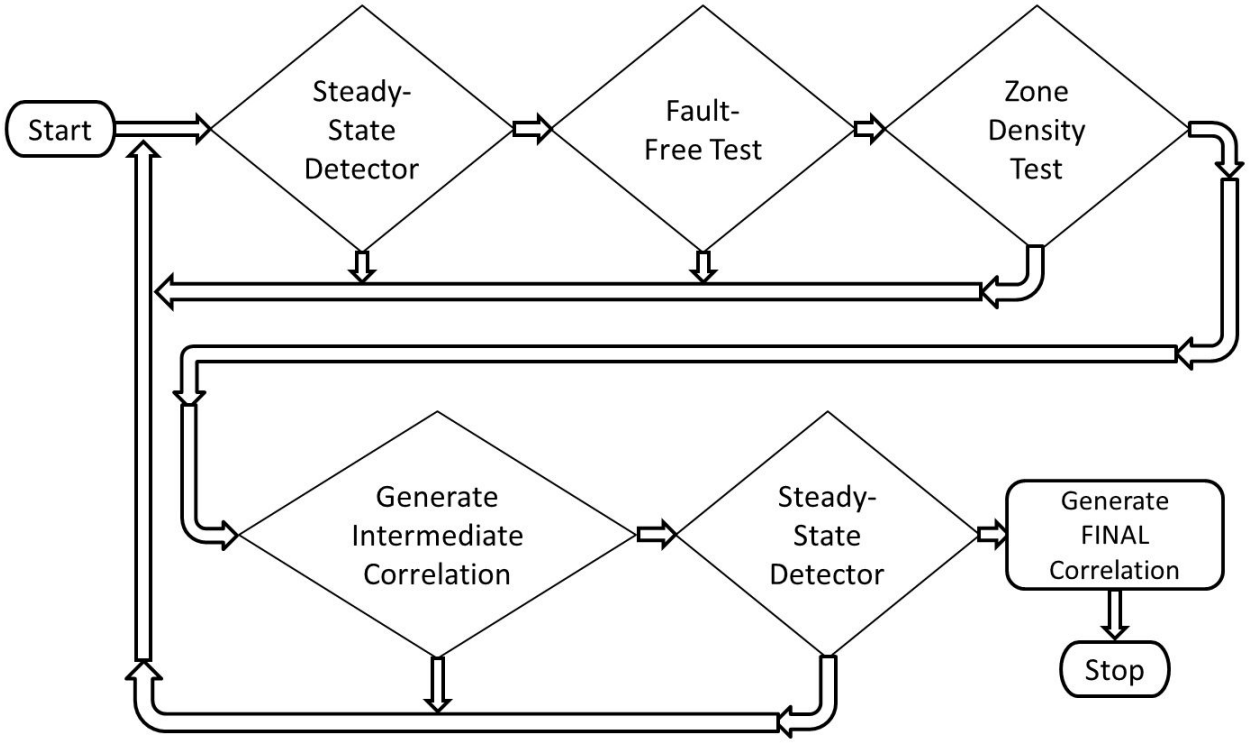

Figure 2.1. General logic for self training

2.3. Measurement Features for Self Training

Following the previous NIST study on residential HP and AC FDD (see Kim et al. 2008b), the three independent features, T_{OD}, T_{ID}, T_{IDP}, and seven dependent features, T_E, T_{SH}, T_C, T_D, T_{SC}, ΔT_{EA}, ΔT_{CA} were chosen for self training (Table 2.1). The value of the seven dependent features can be

correlated as functions of the three independent features within the three-dimensional operating data domain.

Table 2.1. Measurement features for self training

Independent Features (operating conditions)		Dependent Features (FDD features)	
Outdoor dry-bulb temperature	T_{OD}	Evaporator exit refrigerant saturation temperature	T_E
Indoor dry-bulb temperature	T_{ID}	Evaporator exit refrigerant superheat	T_{SH}
Indoor dew point temperature	T_{IDP}	Condenser inlet refrigerant saturation temperature	T_C
		Compressor discharge refrigerant temperature	T_D
		Liquid line refrigerant subcooling temperature	T_{SC}
		Evaporator air temperature change	ΔT_{EA}
		Condenser air temperature change	ΔT_{CA}

3. Self Training Method

3.1. Qualifying Fault-Free Data for the Self Training Dataset

The goal of qualifying the new fault-free data is to develop a uniformly distributed self training dataset for generating fault-free feature models. Figure 3.1 depicts the concept of fault-free data storage in a three-dimensional operating data domain defined in terms of outdoor temperature, indoor temperature, and indoor relative humidity. The domain is divided into "zones" (represented by parallelograms) to facilitate managing the fault-free data distribution. Some measured fault-free data points are indicated by blue points.

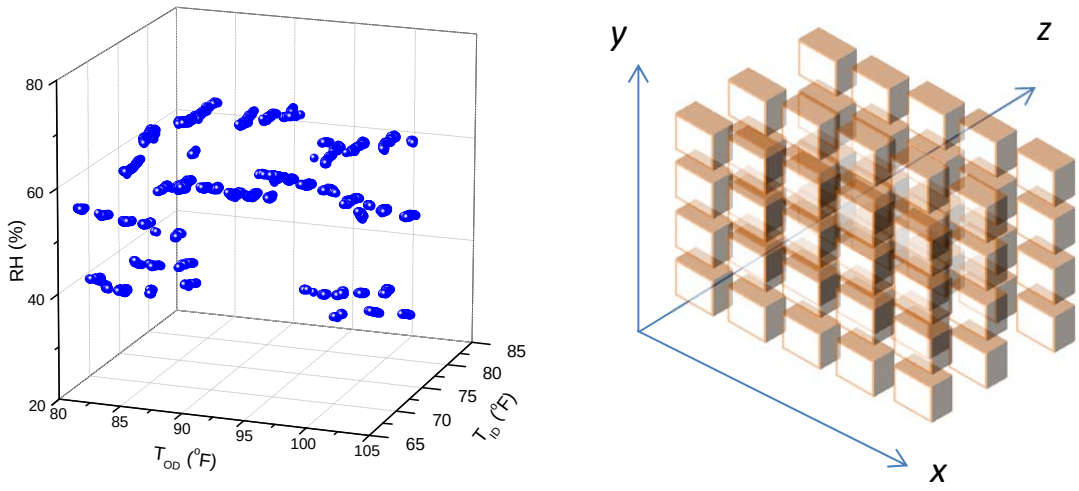

Figure 3.1. Three dimensional operating data domain with sixty zones

The collected data may include multiple data points scattered within the cuboid space of a particular zone. Moreover, storage capacity for data collection in the system has a limitation; therefore, some means of keeping only the best data in a zone must be implemented. To do this zone housekeeping, the concept of zone density (ZD) is introduced to manage and weight the data efficiently. Figure 3.2 shows the concept of a spherical data filter within six, three dimensional cuboid zones, but reduced to two dimensions for clarity of illustration.

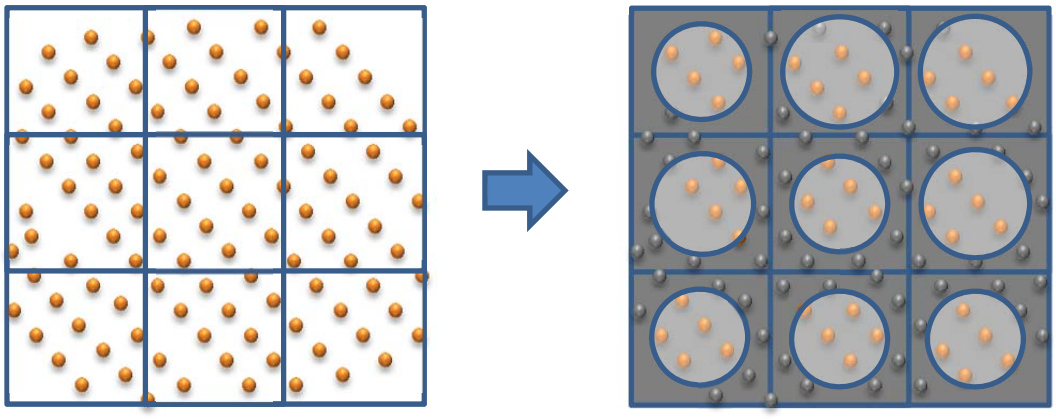

Illustration of data domain ***Application of data filter,* ZD=5**

Figure 3.2. Concept of zone density

To reduce the numerical and dimensional complexity of calculating the spherical radius within the cuboids, the axial dimensions (x,y,z = T_{OD}, T_{ID}, T_{IDP}) are normalized to create a unit cube with

each side having unit area (i.e., 1x1x1). Only data within the sphere are selected, and of the selected data, the data closest to the center are ranked as being higher quality and are selected for storage. Data storage demands are reduced by imposing a zone density (ZD) limit which means that only a specified number of data points, closest to the center of each sphere, are kept. Figure 3.2 shows a ZD equal to 5; any new data within a zone will only be accepted if its distance, *d*, is less than the maximum data point distance occurring in that zone. The distance from the center of the sphere to a data point can be easily calculated as shown in Equation 3.1 and Figure 3.3a.

$$d = \sqrt{(0.5-x)^2 + (0.5-y)^2 + (0.5-z)^2} \tag{3.1}$$

The maximum number of data points in a zone can be adjusted using the zone density concept (Figure 3.3b). A ZD of *m* is defined as the selection of the closest *m* data points from the center in each zone. For example, the allowable data number decreases with the decrease of ZD as shown in Figure 3.3b. In this study, a ZD from 100 to 1 was applied and tested in the self training FDD logic.

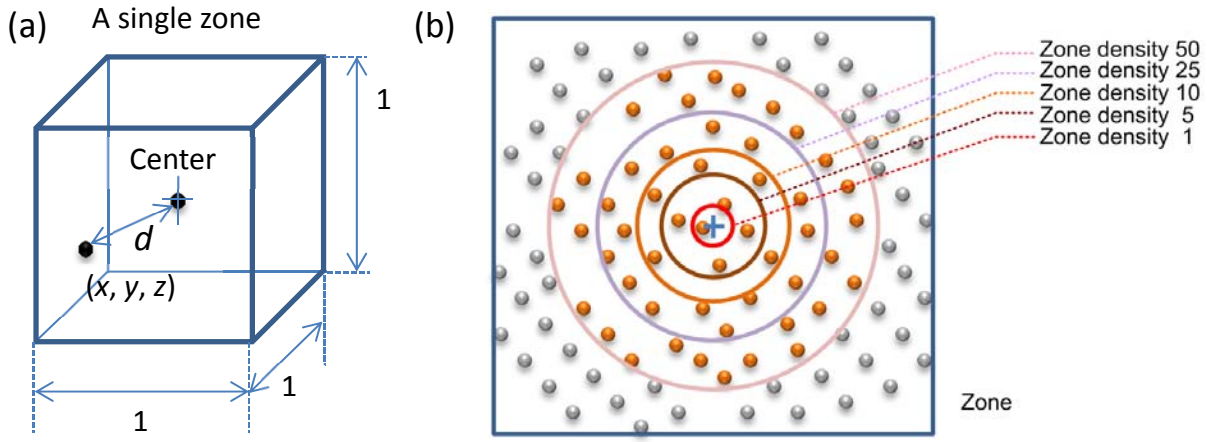

Figure 3.3. Concept of zone density: (a) data distance "*d*" from zone center and (b) various zone densities

3.2. Domain Coverage Rate

Before a fault-free dataset is used to develop models for fault-free features, some numerical criterion needs to be established to assess the quality and extent of the dataset. Preferably, each zone should contain data to avoid extrapolation. According to Braun and Li (2001), the predictions in case of extrapolation showed a deviation 3 to 10 times larger than those predicted by interpolation. Ideally, each zone should contain the same number of data points located close to the center.

For the purpose of rating the extent of the fault-free dataset, the concept of Domain Coverage Rate (DCR) is introduced, which is the ratio of the number of zones with at least one fault-free data point to the total number of zones within the operational data domain. The calculation of the DCR is shown by Equations 3.2 and 3.3. If all zones contain at least one data point then the DCR would equal 100 %.

$$Index_i = \begin{cases} 1 \text{ if data found in i}_{\text{th}} \text{ zone} \\ 0 \text{ if data not found in i}_{\text{th}} \text{ zone} \end{cases} \tag{3.2}$$

$$\text{DCR} = \frac{1}{n}\sum_{i=1}^{n} Index_i \tag{3.3}$$

where *n* is the total number of zones.

3.3 Fault-Free Models

Once the domain coverage rate reaches a specified maximum level, the self training module will correlate the data within all zones using the chosen fault-free model form. The following sections evaluate the performance of several fault-free model forms developed from cooling mode laboratory test data previously acquired for an air-source residential heat pump.

3.3.1. Multivariable Polynomial Regression Models

Multivariable Polynomial Regression (MPR) models have been widely applied as fault-free models [(Li and Braun, 2003), (Braun and Li, 2001), (Kim et al., 2008b), (Heo et al., 2012)] due to their simple structure and ease of programming. They belong to the "black-box" category of models, which do not consider the physics of the system and require a large dataset to accurately predict system performance. The higher order MPR models offer better accuracy of prediction; however, excessive polynomial order for a relatively small database may worsen data interpolation.

Equations 3.4, 3.5, and 3.6 show the general form of the regressed equations for features as 1st, 2nd, and 3rd order MPR models, respectively.

$$\phi^{(1)}_{feature} = a_0 + a_1 T_{OD} + a_2 T_{ID} + a_3 T_{IDP} \tag{3.4}$$

$$\phi^{(2)}_{feature} = \phi^{(1)}_{feature} + a_4 T_{OD} T_{ID} + a_5 T_{ID} T_{IDP} + a_6 T_{IDP} T_{OD} + a_7 T^2_{OD} + a_8 T^2_{ID} + a_9 T^2_{IDP} \tag{3.5}$$

$$\begin{aligned} \phi^{(3)}_{feature} = \phi^{(2)}_{feature} &+ a_{10} T^3_{OD} + a_{11} T^3_{ID} + a_{12} T^3_{IDP} + a_{13} T_{OD} T_{ID} T_{IDP} + a_{14} T^2_{OD} T_{ID} \\ &+ a_{15} T^2_{OD} T_{IDP} + a_{16} T^2_{ID} T_{OD} + a_{17} T^2_{ID} T_{IDP} + a_{18} T^2_{IDP} T_{OD} + a_{19} T^2_{IDP} T_{ID} \end{aligned} \tag{3.6}$$

3.3.2. Artificial Neural Network Models

An Artificial Neural Network (ANN) model was developed for the seven dependent features. The relationship between the three independent variables and seven dependent features is "learned" by an artificial neural network using a back propagation algorithm. The ANN test module was developed based on the sample code presented by Frenz (2002). The fault-free data are used as targets for the back propagation learning.

Figure 3.4 shows the structure of the 3-layer ANN(3x3x1), which has three input variables (T_{OD}, T_{ID}, and T_{IDP}), one hidden layer, and one output. In general, a form of the sigmoid function is used as the activation function in the nodes of the hidden layer. The weight coefficients and offsets (or bias values) are learned using a momentum back propagation algorithm through more than 10 000 iterations (Frenz, 2002).

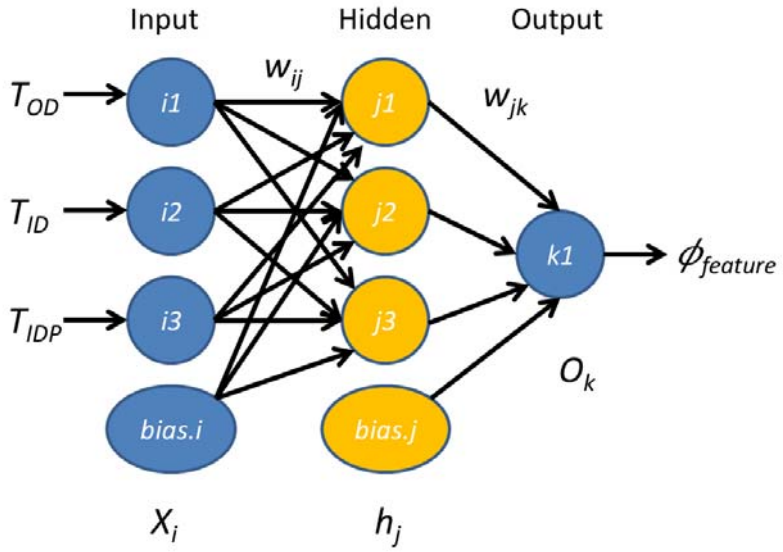

Figure 3.4. Artificial neural network structure (3x3x1)

Each hidden layer neuron is connected to every input neuron and each individual hidden layer neuron receives the sum of the weighted input neuron values as given in Equation 3.7. X_i represents the input neuron values (T_{OD}, T_{ID}, and T_{IDP}) and w_{ij} represents the weights connecting the input neurons to the hidden layer neurons. In a similar way, the output layer neurons are determined as given in Equation 3.8. Bipolar sigmoid function was applied to layer transfer function as given in Equation 3.9.

$$h_{in.j} = h_{\text{bias.i}} + \sum_{i=1}^{n} X_i w_{ij} \quad , \quad h_{out.j} = trans\,(h_{in.j}) \tag{3.7}$$

$$O_{in.k} = O_{\text{bias.j}} + \sum_{j=1}^{n} h_{out.j} w_{jk} \quad , \; O_{out.k} = trans(O_{in.k}) \tag{3.8}$$

$$trans(x) = \frac{2}{1+e^{-x}} - 1 \text{ (bipolar sigmoid)} \tag{3.9}$$

The back-propagation process utilizes a gradient descent algorithm that seeks to minimize the errors of the values that are output from the neural network. The weight and bias update equations including the learning rate (α) and momentum terms (μ) are given in Equations 3.10 through 3.13. The learning rate fragments the weight/bias adjustment taken in each training iteration. The smaller the value of alpha, the longer a network takes to train, but the smaller alpha reduces fluctuations in the weight variation from iteration to iteration and generally produces smaller errors. Momentum is added to the weight adjustment equations (Equations 3.10 and 3.12), which enables the weight to change in response to the current gradient step. Delta (δ) is calculated by multiplying the difference between the target value and output value by the derivative of the activation function (Equation 3.14). Here *t* represents the current set of weights/biases, *t*-1 the previous set, and *t*+1 the new set being calculated.

$$w_{jk}(t+1) = w_{jk}(t) + \alpha\delta \cdot h_{out.j} + \mu(w_{jk}(t) - w_{jk}(t-1)) \tag{3.10}$$

$$O_{bias.k}(t+1) = O_{bias.k}(t) + \alpha\delta + \mu(O_{bias.k}(t) - O_{bias.k}(t-1)) \tag{3.11}$$

$$w_{ij}(t+1) = w_{ij}(t) + \alpha\delta \cdot X_i + \mu(w_{ij}(t) - w_{ij}(t-1)) \tag{3.12}$$

$$h_{bias.j}(t+1) = h_{bias.j}(t) + \alpha\delta + \mu(h_{bias.j}(t) - h_{bias.j}(t-1)) \tag{3.13}$$

$$\delta = \frac{1}{2}\left(1 + trans(O_{in})\right) \cdot \left(1 - trans(O_{in}) \cdot (O_{target} - O_{out})\right) \tag{3.14}$$

The standard deviation (σ) of the ANN model was investigated with the variation of the learning rate, alpha (α), momentum (μ), maximum iteration number, and number of hidden layers, as shown in Figure 3.5. The ANN model's performance was the most sensitive with learning rate (α) and iteration number, which were optimized at 0.001 and 10 000, respectively. The ANN model's performance improved with the increase of the momentum term. However with the momentum term greater than 0.1, the ANN model's performance decreased due to too large of a gradient for training. If the number of hidden layers increased, the total number of variables for modeling also increased. As a result, the ANN model with three layers showed the best performance.

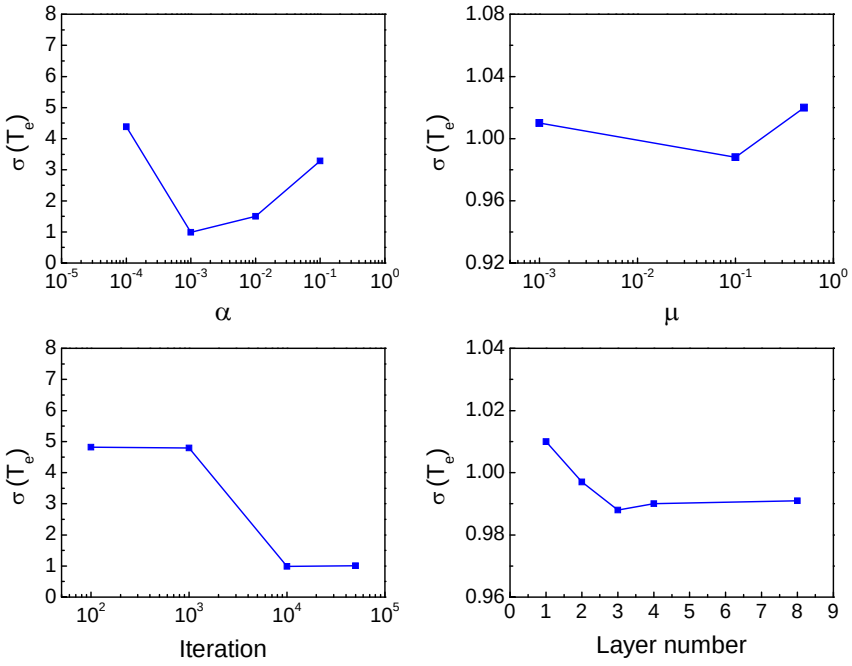

Figure 3.5. Operating factor optimization for the ANN model

3.3.3. Combined ANN-MPR Models

Used alone, the ANN model showed good interpolation performance, poor extrapolation performance, and relatively long times required for training. The low-order MPR model had relatively good extrapolation performance, low interpolation performance, and very fast training times. In order to combine the strengths of the ANN and MPR models, a combined model was designed as illustrated by Braun and Li (2001).

In this study, the first and second order MPR models and the ANN (3x3x1) model were applied in the combined model. First, the MPR model was regressed with the training data, and then the residuals between the model output and the training data were fit with an ANN. This combined model is calculated as given in Equation 3.15.

$$\phi_{Combine} = \phi_{MPR} + \phi_{ANN} \tag{3.15}$$

4. Self Training Implementation

4.1. Experimental Setup and Fault-Free Data Collection

To test and validate the self training scheme presented in the previous sections, we developed a fault-free database with laboratory data taken on an R410A, 8.8 kW split heat pump operating in the cooling mode. The unit had a Seasonal Energy Efficiency Ratio (SEER) of 13 (AHRI, 2008).

The unit consisted of an indoor fan-coil section, outdoor section with a scroll compressor, cooling and heating mode thermostatic expansion valves (TXV), and connecting tubing. Both the indoor and outdoor air-to-refrigerant heat exchangers were of the finned-tube type. The unit was installed in environmental chambers and charged with refrigerant according to the manufacturer's specifications. Figure 4.1 shows a schematic of the experimental setup indicating the measurement locations. On the refrigerant side, pressure transducers and T-type thermocouple probes were attached at the inlet and exit of every component of the system. The refrigerant mass flow rate was measured using a Coriolis flow meter. The air enthalpy method served as the primary measurement of the system capacity, and the refrigerant enthalpy method served as the secondary measurement. These two measurements always agreed within 5 %. Uncertainties of the major quantities measured during this work are summarized in Table 4.1. Detailed specifications of the test rig including indoor ductwork, dimensions, data acquisition, measurement uncertainty, and instrumentation is described in Kim et al. (2006).

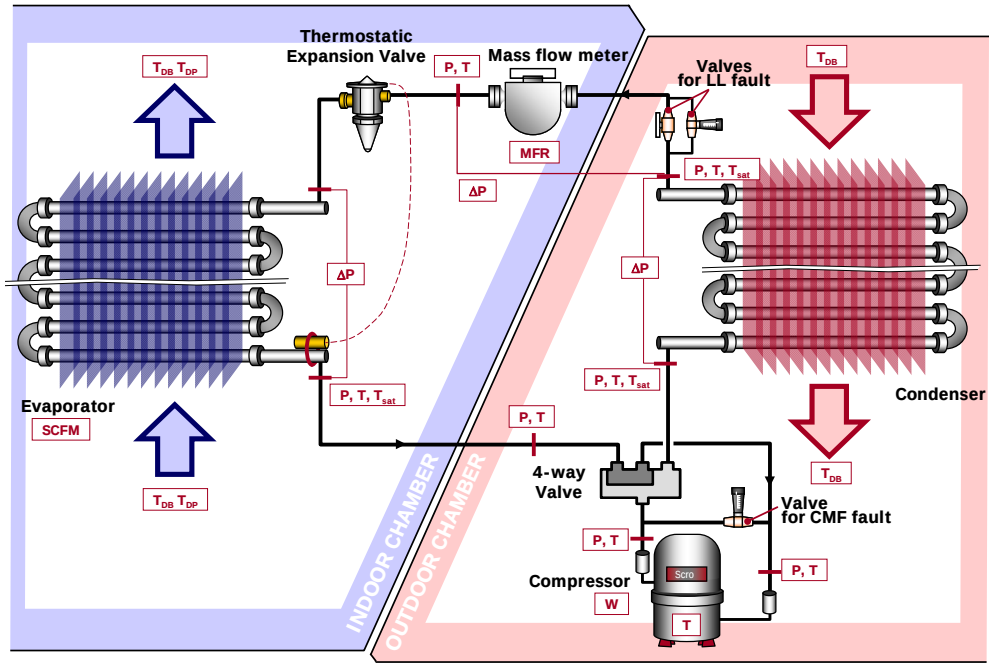

Figure 4.1. Schematic diagram of the experimental setup (Kim et al., 2006)

To implement the most efficient test procedure, outdoor temperature was fixed at one of four values, the addition of steam to the indoor chamber was set at one of several discrete levels by modulating a steam valve, and the indoor dry-bulb temperature was changed over the desired operating range by energizing 10 heaters sequentially. From the total number of 10 409 recorded data scans, 5830 data sets were allowed by the steady-state detector. The data were recorded every 18 s and filtered through the steady-state detector, which qualified steady-state

data for use in development of the fault-free models for the seven features. In this process, instability of the system due to on-off transients and rapid load changes was filtered out by the steady-state detector. From the total number of 10 409 recorded datasets, 5830 datasets were kept by the steady-state detector.

Table 4.2 shows operating conditions for the fault-free tests. The four outdoor temperatures were maintained within ±0.5 °F. For the indoor conditions, the amount of steam introduced to the indoor chamber was fixed such that the humidity ratio varied from 0.0037 to 0.0168. Data were recorded, every 18 s, as indoor dry-bulb temperature varied from 59.5 °F to 93.0 °F. The range of operating conditions for which data were collected defines the applicable limits for the FDD scheme.

Table 4.1. Measurement uncertainties

Measurement	Range	Uncertainty at a 95 % Confidence Level
Individual temperature	-0.4 °F to 199.4 °F	±0.54 °F
Temperature difference	0 °F to 50.4 °F	±0.54 °F
Air nozzle pressure drop	0 Pa to 1245 Pa	±1.0 Pa
Refrigerant mass flow rate	0 kg/h to 544 kg/h	±1.0 %
Dew point temperature	-0.4 °F to 100.4 °F	±0.72 °F
Dry-bulb temperature	-0.4 °F to 104 °F	±0.72 °F
Total cooling capacity	3 kW to 11 kW	±4.0 %
COP	2.5 to 6.0	±5.5 %

Table 4.2. Operating conditions for fault-free tests

Outdoor dry-bulb temp. °F	82, 90, 95, 100
Indoor dry-bulb temp. °F	59.5 to 93
Indoor humidity ratio	0.0037 to 0.0168

If we assume that the data distribution is similar to that of a field-installed, real system, the DCR can be calculated based on the accumulated dataset as introduced in Equations 3.2 and 3.3. Figure 4.2 shows the fault-free data distribution with increments of the domain coverage rate. DCR of 20 %, 40 %, 60 %, and 73 % were fulfilled when the accumulated data points reached 2104, 2830, 4211, and 5830, respectively. The datasets corresponding to these four DCRs were used for the self training of different fault-free models.

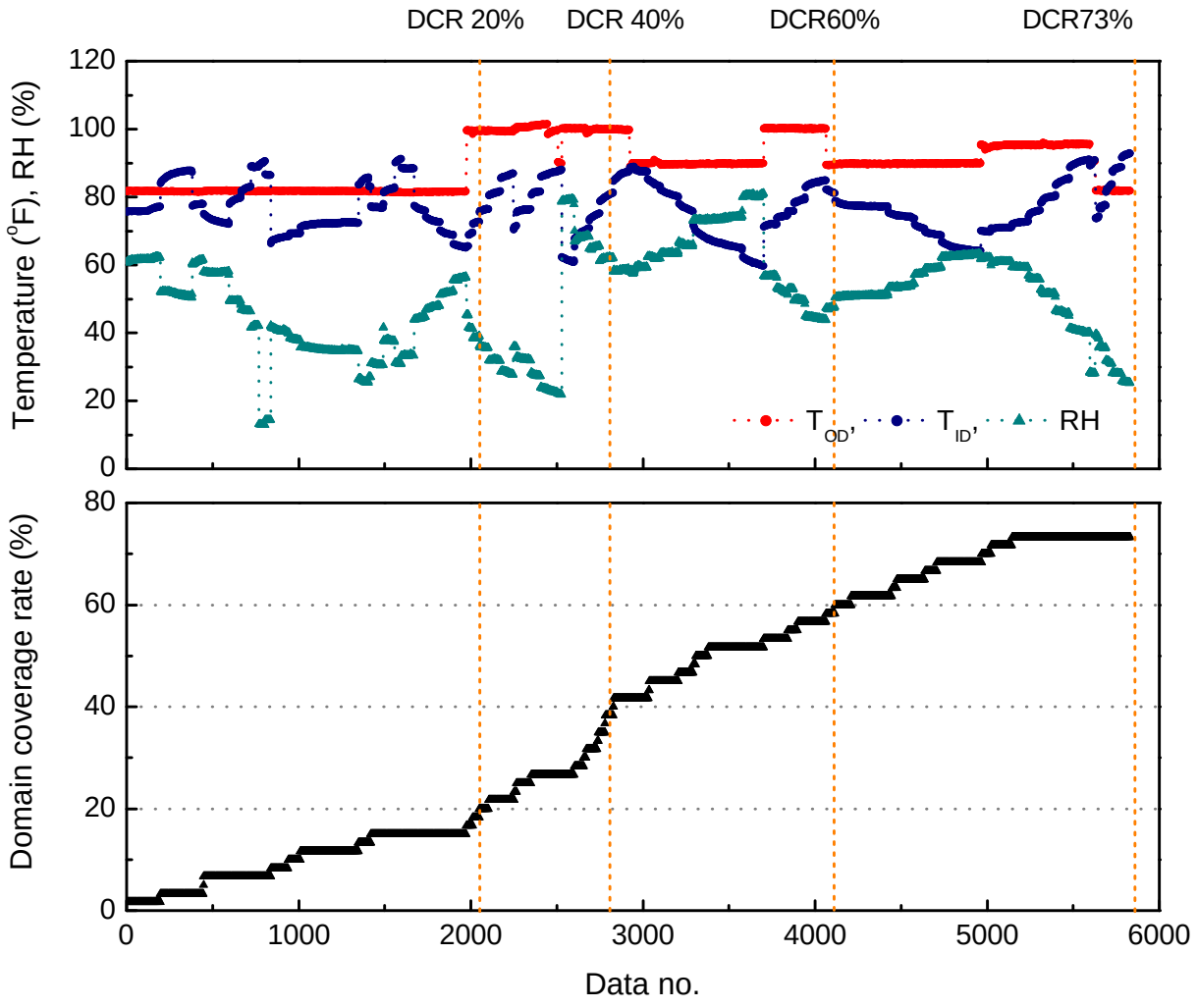

Figure 4.2. Test condition data distribution and progression of domain coverage

4.2. Fault-Free Model Performance with the Whole Dataset

Six fault-free model types [MPR(1st order), MPR(2nd order), MPR(3rd order), ANN, and two combined models (MPR(1st order) + ANN, MPR(2nd order) + ANN)] were tested and compared using the entire dataset. Each model's overall performance was evaluated by calculating the standard error, as given in Equation 4.1. The test standard error (TSE) is calculated from the square root of the squared summation of residuals divided by the number of data points, *N*.

$$TSE=\sqrt{\frac{\sum_{i}(x_i-\phi_{i.FF})^2}{N}} \tag{4.1}$$

Among the dependent features, the TSE of T_D and T_C were the highest and the lowest, respectively. The MPR(3rd order) model showed the lowest prediction error, followed by the MPR(2nd order), combined MPR(2nd order)+ANN, combined MPR(1st order)+ANN, and ANN model (Figure 4.3). Therefore, the MPR methods were applied and tested for additional analysis of the self training method.

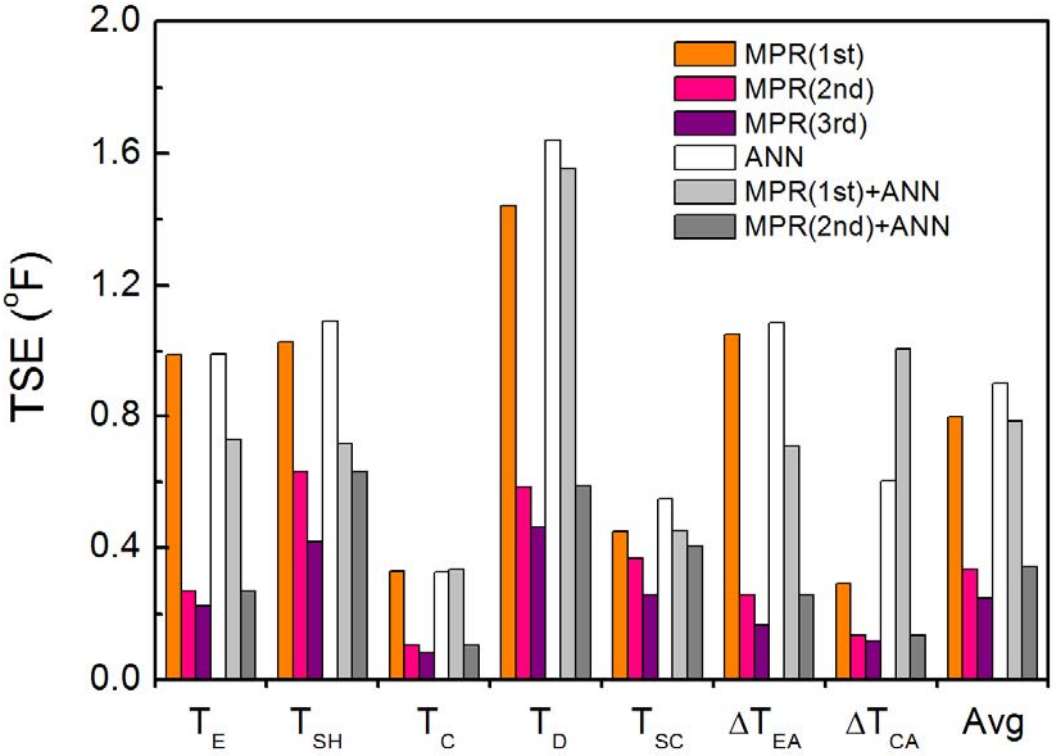

Figure 4.3. Fault-free models performance on the whole dataset

4.3. Fault-Free Model Performance with Different Zone Densities

The zone density (ZD) concept was introduced to limit the data needed to generate a model while collecting data over the predefined range of independent variables. In this section, the prediction performance of the fault-free model was tested with various zone densities. In the process of training, fault-free models were developed based on the data kept at the desired ZD, and then the prediction performance was tested on the filtered dataset in the test range (4627 of the 5830 original points after eliminating repeated tests).

Limiting the zone density produced a smaller dataset of training data; the bigger the zone density number, the larger the training dataset for the training process. When the zone density

decreased from 100 to 10, the data quantity drastically decreased from 2968 to 426 (Figure 4.4). Therefore, as the ZD number decreased, the training speed and data storage compactness also improved due to the smaller dataset. However, too small of a zone density number can decrease the prediction performance.

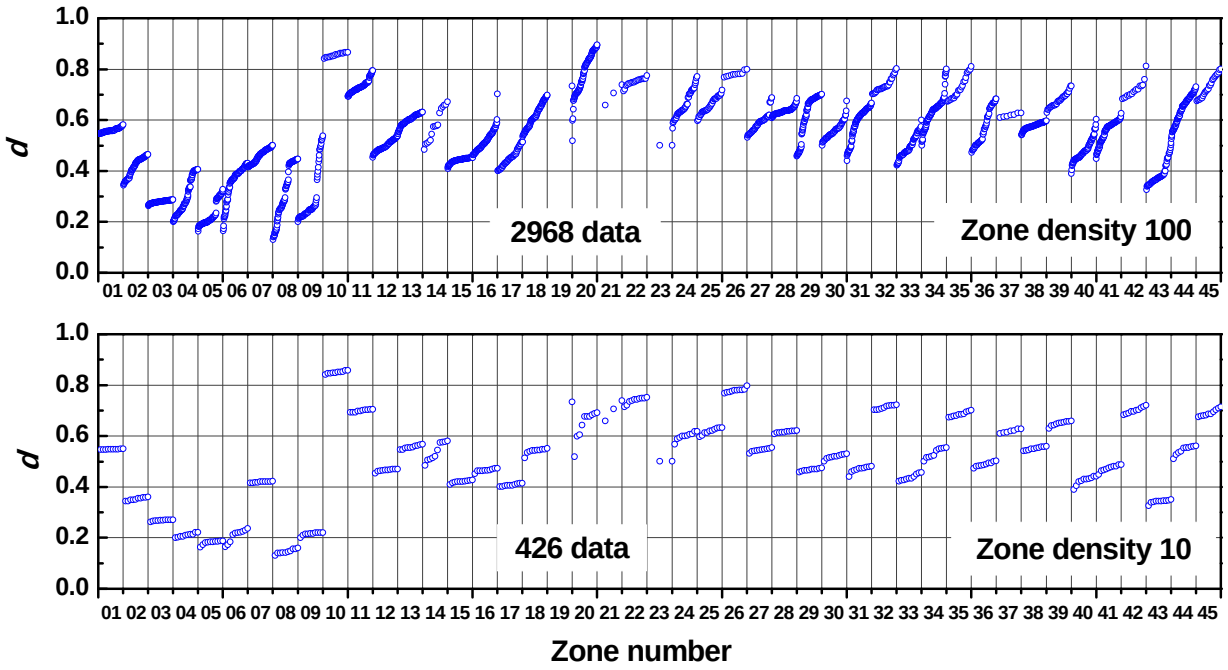

Figure 4.4. Data distance to zone center for different zones for two zone densities

Figure 4.5 shows the standard error of the fault-free model for the seven dependent features with different zone densities. Whereas the standard error for T_E, T_C, ΔT_{EA}, ΔT_{CA} was relatively non-sensitive to the variation of zone density, the standard error for T_{SH}, T_D, and T_{SC} was more rapidly increased with the decrease of zone density. The MPR(3rd order) model was the most sensitive to zone density variation. The MPR(3rd order) model has a relatively large number of coefficients (20) compared to the first order (4) and the second order (10) MPR models, so that it requires abundant data for stable regression. On average, the MPR(3rd order) model showed the lowest standard error followed by the second and the first order MPR models, respectively. At a zone density of 100, the standard error remained at a similar level to the models using all of the data (5830 non-filtered case). When the zone density was less than 25, the MPR(3rd order) model showed similar prediction performance to that of the MPR(2nd order) model. The MPR(3rd order) model with zone density of 100 showed the most stable and best prediction performance.

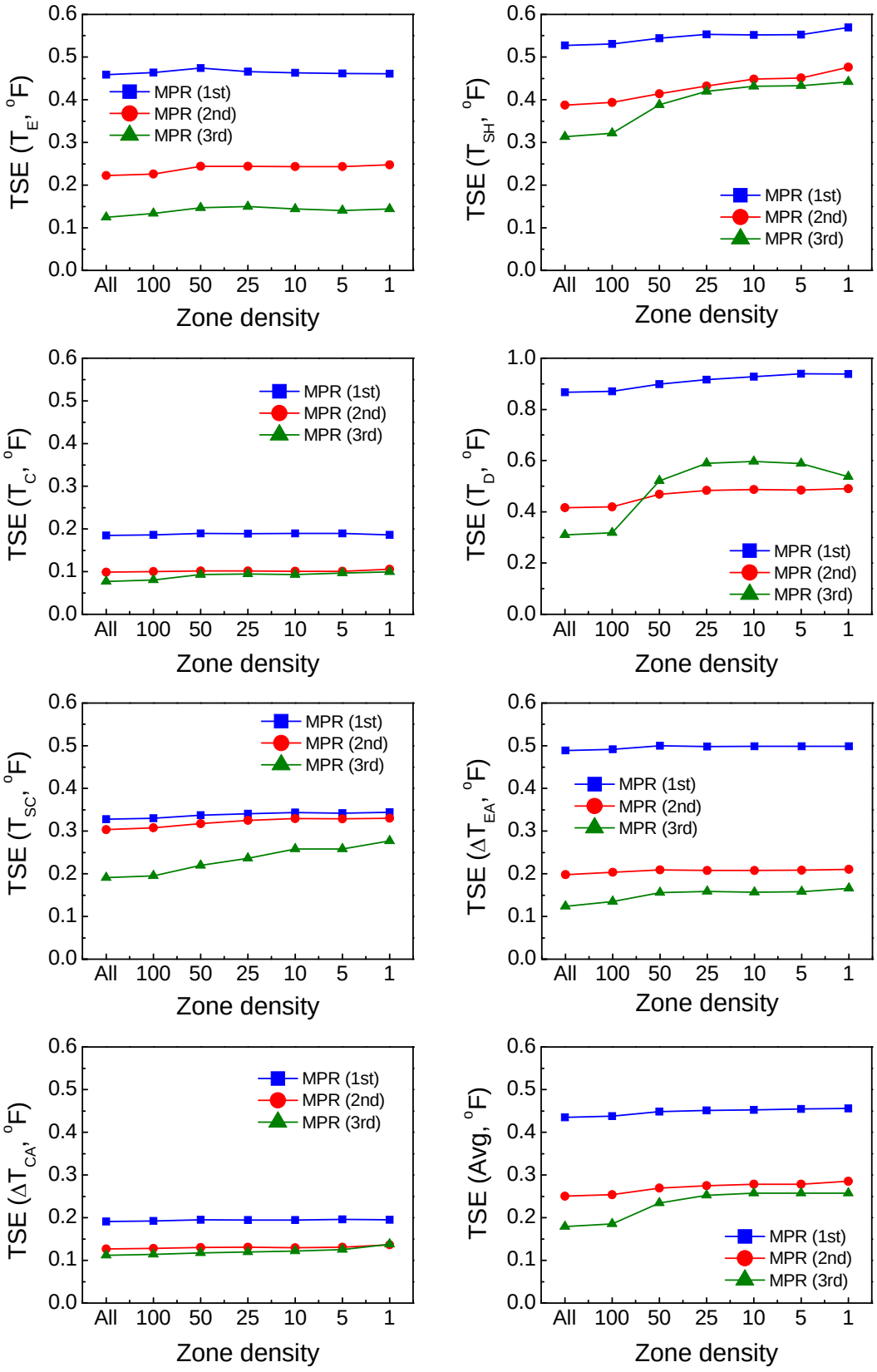

Figure 4.5. Fault-free model performance with zone density (Test Standard Error)

4.4. Fault-Free Model Performance with Different Domain Coverage Rates

Figure 4.6 shows the domain coverage rate as the size of the fault-free dataset increases up to its maximum value of 5380 data points. As the number of accumulated fault-free data points increases, the DCR increases up to 73 %. The figure shows four training ranges corresponding to DCR values of 20 %, 40 %, 60 % and 73 %.

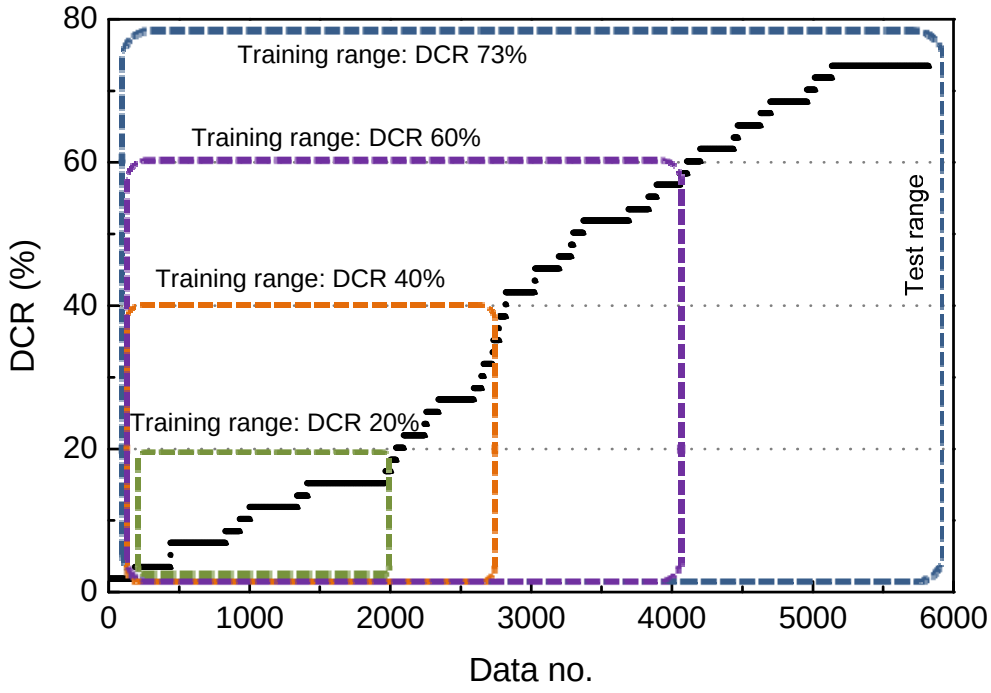

Figure 4.6. Domain coverage rate for different accumulated data quantity

Figure 4.7 shows the standard error of the fault-free models for the seven dependent features as a function of the domain coverage rate. The standard error on all features decreased with an increase in the DCR. The standard error of the MPR(3rd order) model was the most sensitive to DCR variation. In a real system that is collecting training data, when the DCR is low, each feature has a higher likelihood of being estimated by extrapolation using the currently generated fault-free model. In most cases, the first and second order MPR models showed the lowest standard errors at 20 % and 40 % DCR conditions, respectively. The MPR(3rd order) model was the best at 60 % and 73 % DCR. After the DCR reached 40 %, the standard errors of all fault-free feature correlations were less than 1 ^{o}F.

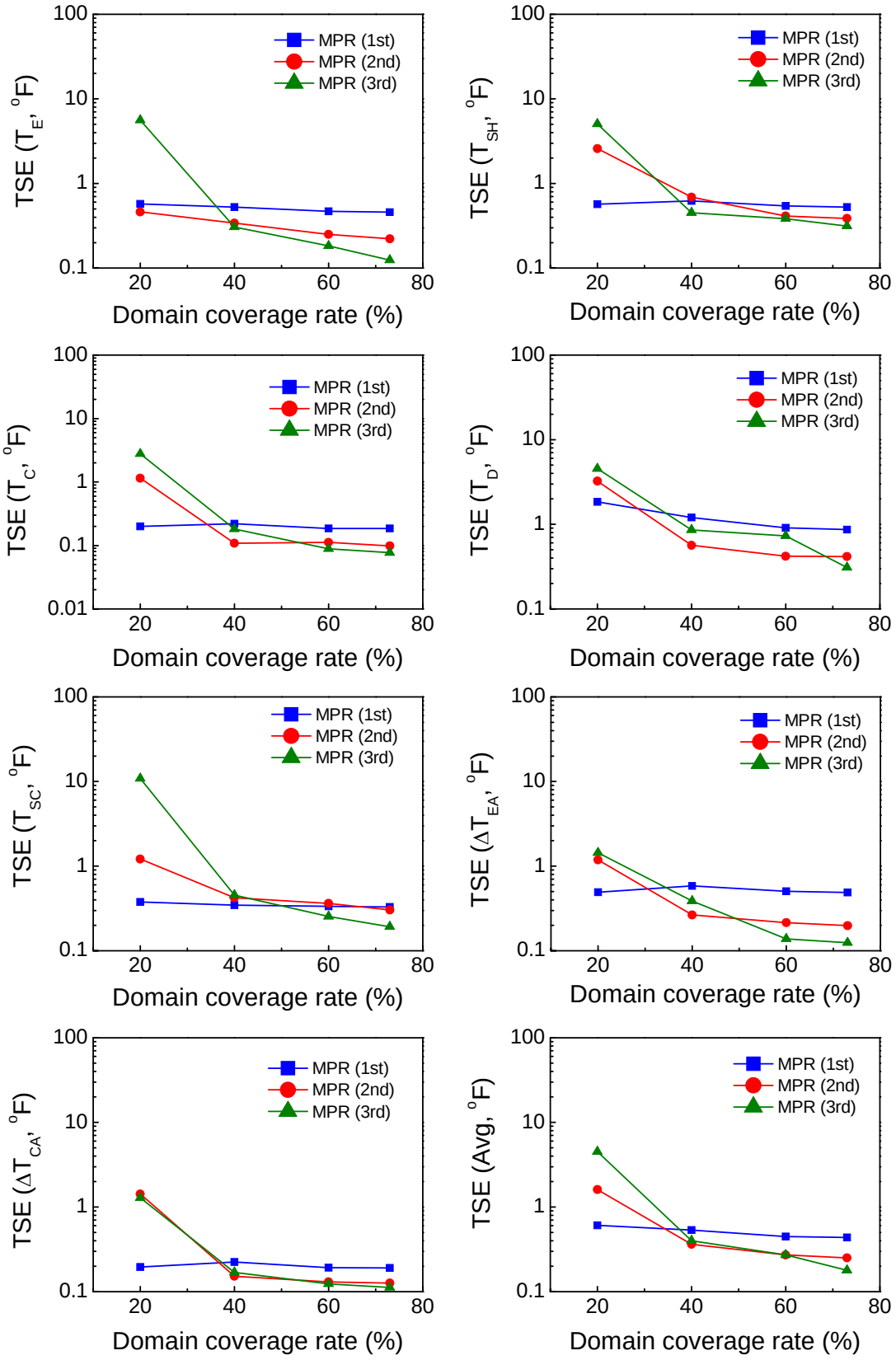

Figure 4.7. Fault-free models performance with domain coverage rate (Test Standard Error)

The above standard error results are consistent with Braun and Li (2001) who commented that the lower the order of the MPR model the better the extrapolation performance, in general. When the DCR is low, each feature has a higher likelihood of being estimated by extrapolation. For models generated at higher DCRs, extrapolation is less likely, and higher-order MPR models are better where interpolation is required.

Figure 4.8 shows TSE of the MPR models for 20 %, 40 %, 60 %, and 73 % DCR as a function of zone density. At a DCR of 20 %, the TSE of MPR(3rd order) and MPR(2nd order) exceeded 4 ^{o}F, and 1 ^{o}F, respectively, with steep increases at low ZD values. For the higher DCRs, the TSE stayed below 1 ^{o}F for all models and ZDs except MPR(3rd order) for 40 % DCR and ZD less than 25. For 60 % and 73 % DCR, all three models performed in a stable fashion smoothly improving predictions as DCR and ZD values increased.

From this analysis, the MPR(1st order) and MPR(2nd order) models are recommendable for the intermediate fault-free models at a DCR of 20 % and 40 %, respectively. After the DCR exceeds 60 %, the MPR(3rd order) model is the most appropriate for the final fault-free model. A ZD between 100 and 50 is recommended for data filtering and storing criteria.

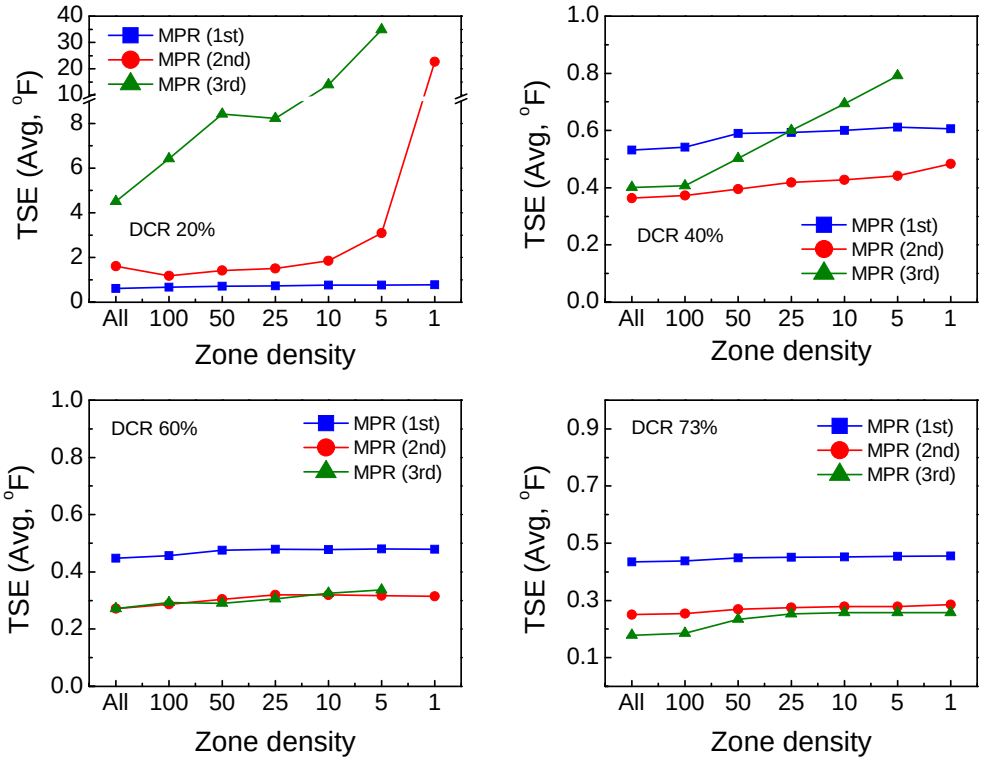

Figure 4.8. Model standard error with zone density at DCR of 20 %, 40 %, 60 %, and 73 %

5. Validation

We tested and validated the self training method by applying the fault-free models developed using the self training scheme to an experimental dataset collected by Kim et al. (2006) on a heat pump operating in the cooling mode. In addition, the FDD performance was compared and analyzed considering different zone densities and domain coverage rates. Successful diagnosis ratio, false alarm, missed detection, and misdiagnosis were calculated and presented to evaluate the overall FDD performance.

5.1. Validation Dataset and Fault Types

The dataset assembled by Kim et al. (2006) includes performance data during fault-free operation (72 points) and with seven faults: compressor valve leakage, improper outdoor air flow, improper indoor air flow, liquid line restriction, refrigerant undercharge, refrigerant overcharge, and non-condensables (84 points) (Table 5.1).

Table 5.1. Definition and range of studied heat pump operational cases

Fault name	Symbol	Definition of fault	Fault range (%)	Temperature range (^{o}F)	Number of points
Fault-free (Normal operation)	FF	-	-	T_{OD}: 80 to 102 T_{ID}: 65 to 85 T_{IDP}: 42 to 85	72
Compressor valve leakage (4 to way valve leakage)	CMF	% reduction in refrigerant flow rate from no-fault value	3 to 40	T_{OD}: 80 to 100 T_{ID}: 70 to 80 T_{IDP}: 50 to 61	16
Reduced outdoor air flow rate (condenser fouling)	CF	% of coil area blocked	10 to 50	T_{OD}: 80 to 100 T_{ID}: 70 to 80 T_{IDP}: 50 to 61	13
Improper indoor air flow rate (evaporator fouling)	EF	% below specified air flow rate	6 to 35	T_{OD}: 80 to 100 T_{ID}: 70 to 80 T_{IDP}: 42 to 61	19
Liquid line restriction	LL	% change from no-fault pressure drop from liquid line service valve to indoor TXV inlet	10 to 32	T_{OD}: 80 to 100 T_{ID}: 70 to 80 T_{IDP}: 50 to 61	6

Refrigerant undercharge	UC	% mass below correct (no-fault) charge	10 to 30	T_{OD}: 80 to 100 T_{ID}: 70 to 80 T_{IDP}: 50 to 61	12
Refrigerant overcharge	OC	% mass above correct (no-fault) charge	10 to 30	T_{OD}: 80 to 100 T_{ID}: 70 to 80 T_{IDP}: 50 to 61	12
Presence of non-condensable gases	NC	% of pressure in evacuated indoor section and line set, due to non-condensable gas, with respect to atmospheric pressure	10 to 20	T_{OD}: 80 to 100 T_{ID}: 70 to 80 T_{IDP}: 50 to 61	6

5.2. Fault Detection and Diagnostic Method

When the system is operating with a fault, it is expected that feature temperatures willdeviate from their normal, fault-free values. An individual feature's deviation could be negative, positive, or "neutral" (close to the fault-free value within a pre-defined threshold); collectively, the feature's deviations (or residuals) form a pattern, which is unique for a given fault. To detect and diagnose the fault, a statistical rule-based classification is performed by calculating the probability of the various fault-types based on the decision rules defined within a rule-based chart's predefined fault patterns. A set of measurement features can be regarded as a multi-dimensional Gaussian probability distribution. With the assumption that each dimension is independent, each of the three "class" problems (negative, positive, or neutral) can be represented by a simple normal (Gaussian) distribution rather than a more complicated distribution with multiple degrees of freedom and dependencies (Rossi et al., 1995, Kim et al., 2008b). The probability of the k^{th} fault corresponding to the set of m statistically independent variables (***X***, *our features*) is given by Equation 5.1, where $P(C_{ik}|X_i)$ denotes the individual probability of case variable C (negative, positive, or neutral) for the i^{th} feature with the k^{th} fault type. Since the features are assumed to be independent, the total conditional probability, $P(F_k|\boldsymbol{X})$, can be obtained by the multiplication of the individual probabilities.

$$P(F_k|\mathbf{X}) = P(C_{1k}|X_1)\cdot P(C_{2k}|X_2)\cdots P(C_{ik}|X_i) = \prod_{i=1}^{m} P(C_{ik}|X_i) \tag{5.1}$$

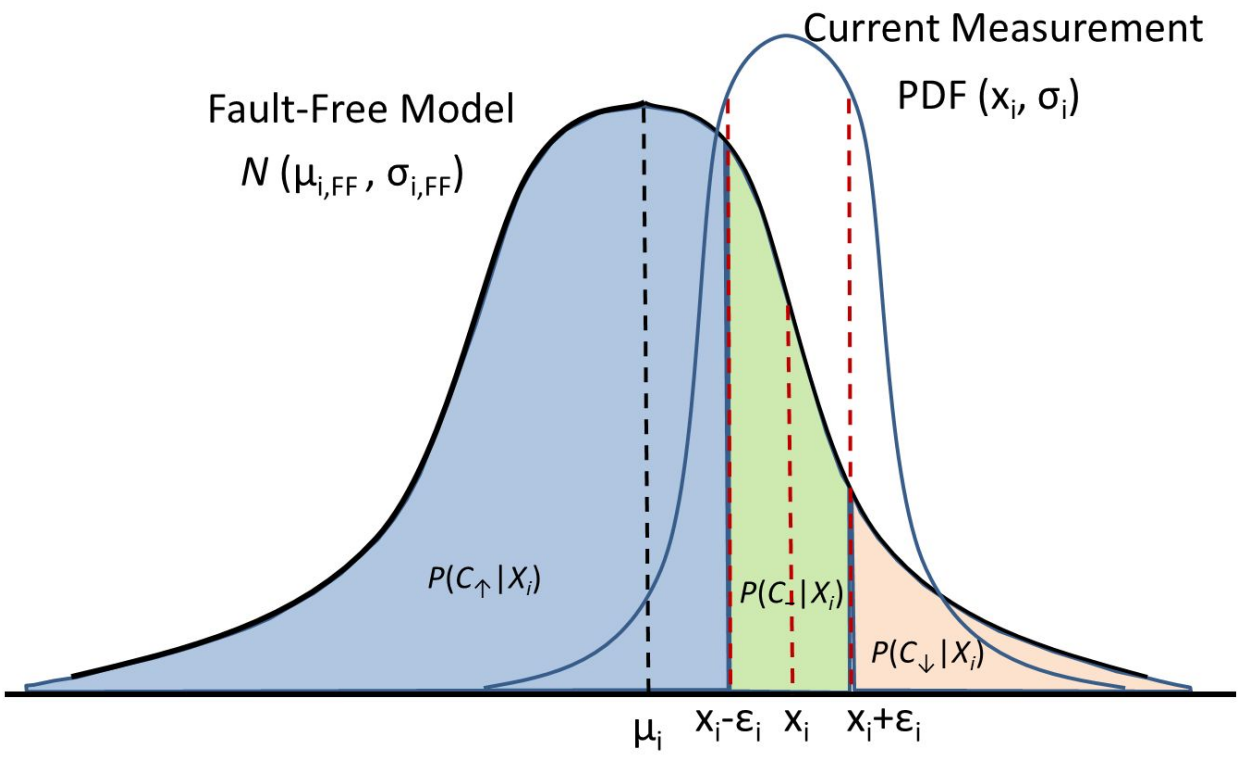

Figure 5.1. Probability for three measurement residual cases of positive, neutral, and negative

In Figure 5.1, the three differently cross-hatched areas under the Normal Distribution, $N(\mu_{i,FF}, \sigma_{i,FF})$, represents the probability of the current measurement (or predicted value), represented by a second normal distribution, $PDF(x_i, \sigma_i)$, being lower, higher, or relatively close (neutral) to the predicted fault-free model's value; if the conditions are fault-free, the difference in the measured and predicted value, the residual, $r_i = x_i - \mu_{i,FF}$, will equal zero. In order to locate the position of the current measurement under the normal distribution, we must convert the currently measured value to its standard form; we must represent the current measurement as some number of fault-free model standard deviations from the mean value of the fault-free normal distribution (the currently predicted value). This standardization is often called the z-value. Therefore the z-value for the current measurement, z_i, is defined by our residual and the standard deviation of the fault-free model as shown in Equation 5.2.

$$z_i = \frac{x_i - \mu_{i.FF}}{\sigma_{i,FF}} = \frac{r_i}{\sigma_{i,FF}} \tag{5.2}$$

Using the assumption of independent, normally distributed FDD features, the area under the normal distribution, $N(\mu_{i,FF}, \sigma_{i,FF})$, must be determined in order to place a numerical value on the probability. This integral is represented by the cumulative distribution function, $\Phi(x)$, Equation

5.3, of the standard normal distribution (a normal distribution with a mean of zero and standard deviation of 1, $N(0,1)$).

$$\emptyset(x) = \frac{1}{2} + \frac{1}{2} erf\left(\frac{x}{\sqrt{2}}\right) \tag{5.3}$$

The cumulative distribution function describes the probability of a real number value with a given probability distribution function, X ∈ $PDF(x_i, \sigma_i)$, having a value less than or equal to a given value, a. This can be re-stated as Equation 5.4.

$$\emptyset(a) = P(X \leq a) \tag{5.4}$$

This also leads to the probability of X lying within the semi-closed interval (a, b] or being greater than some value, b, Equations 5.5 and 5.6, respectively.

$$P(a < X \leq b) = \emptyset(b) - \emptyset(a) \tag{5.5}$$

$$P(X > b) = 1 - \emptyset(b) \tag{5.6}$$

For the purposes of FDD, we would like to know whether the residual, r_i, is positive, negative, or insignificant (i.e., within $\pm\varepsilon_i$ (neutral threshold) of the FF model predicted value, $\mu_{i,FF}$). In order to use the cumulative distribution function, we must standardize the intervals around the currently measured value, $x_i \pm \varepsilon_i$, as a multiple of the FF model standard deviation; therefore we "standardize" ε_i as being s number of FF model standard deviations as shown in Equation 5.7; s is the "standardized" width of the neutral threshold (s>0). The standardized representation of the residual and three possible cases (positive, negative, and neutral) are shown in Figure 5.2.

$$\varepsilon_i = s\sigma_{i,FF} \text{ or } s = \frac{\varepsilon_i}{\sigma_{i,FF}} \tag{5.7}$$

Now we may use Equation 5.6 to determine the probability of the residual being greater than $+\varepsilon_i$, the negative residual case;

$$P(C_{\downarrow}|X_i) = P(z_i > (z_i + s)) = 1 - \emptyset(z_i + s) \tag{5.8}$$

Less than or equal to $-\varepsilon_i$, the positive residual case using Equation 5.4;

$$P(C_{\uparrow}|X_i) = P(z_i \leq (z_i - s)) = \emptyset(z_i - s) \tag{5.9}$$

Or in the neutral interval of $\pm\varepsilon_i$ using Equation 5.5;

$$P(C_{-}|X_i) = P((z_i - s) < z_i \leq (z_i + s)) = \emptyset(z_i + s) - \emptyset(z_i - s) \tag{5.10}$$

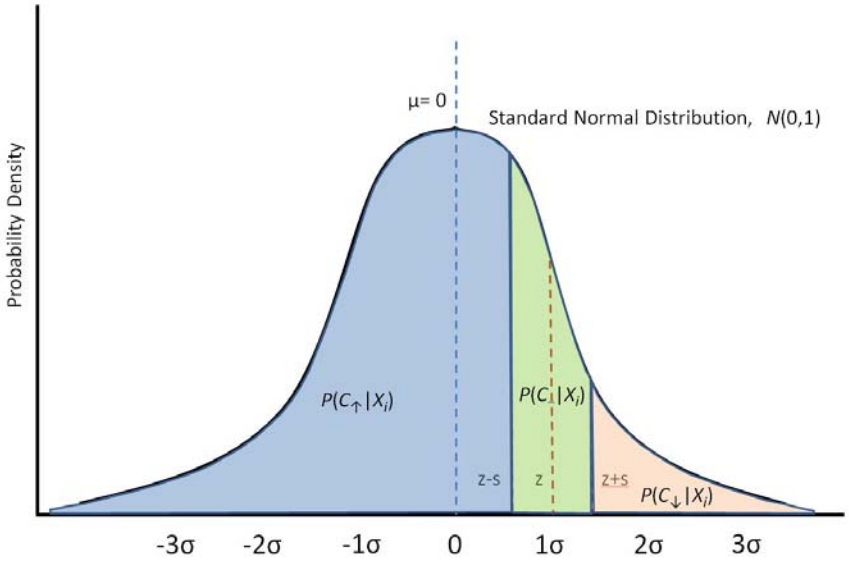

Figure 5.2. Standard normal distribution showing the current measurements z-value and standardized neutral threshold, s

The summation of probabilities calculated in Equations 5.8 to 5.10 equals unity, Equation 5.11, since the integral of any PDFs from –∞ to +∞ must equal one by definition.

$$P(C_{\downarrow}|X_i) + P(C_{\uparrow}|X_i) + P(C_{-}|X_i) = 1 \tag{5.11}$$

When the fault level increases, the residual between the measured data and predicted data may increase, decrease, or remain relatively unchanged. Figure 5.3 shows the residual pattern analysis results for the seven studied faults which were used to generate a rule-based chart. Due to the careful selection of the most sensitive (rapidly changing) features for a given fault type, the feature patterns were quite different for all fault types, and each pattern (positive, negative, and neutral) for a given fault is the template for the calculation of fault probability in Equation 5.1. For example, the probability of a CMF fault (valve leakage) can be calculated by the multiplication of the conditional probabilities of the residuals having the following pattern: T_E (positive), T_{SH} (neutral), T_C (negative), T_D (positive), T_{SC} (negative), ΔT_{EA} (negative), and ΔT_{CA} (negative), as shown in Equation 5.12.

$$\begin{aligned} P(F_{CMF}|\mathbf{X}) = {} & P(C_{\uparrow}|T_E) \cdot P(C_{-}|T_{SH}) \cdot P(C_{\downarrow}|T_C) \cdot P(C_{\uparrow}|T_D) \cdot P(C_{\downarrow}|T_{SC}) \\ & \cdot P(C_{\downarrow}|\Delta T_{EA}) \cdot P(C_{\downarrow}|\Delta T_{CA}) \end{aligned} \tag{5.12}$$

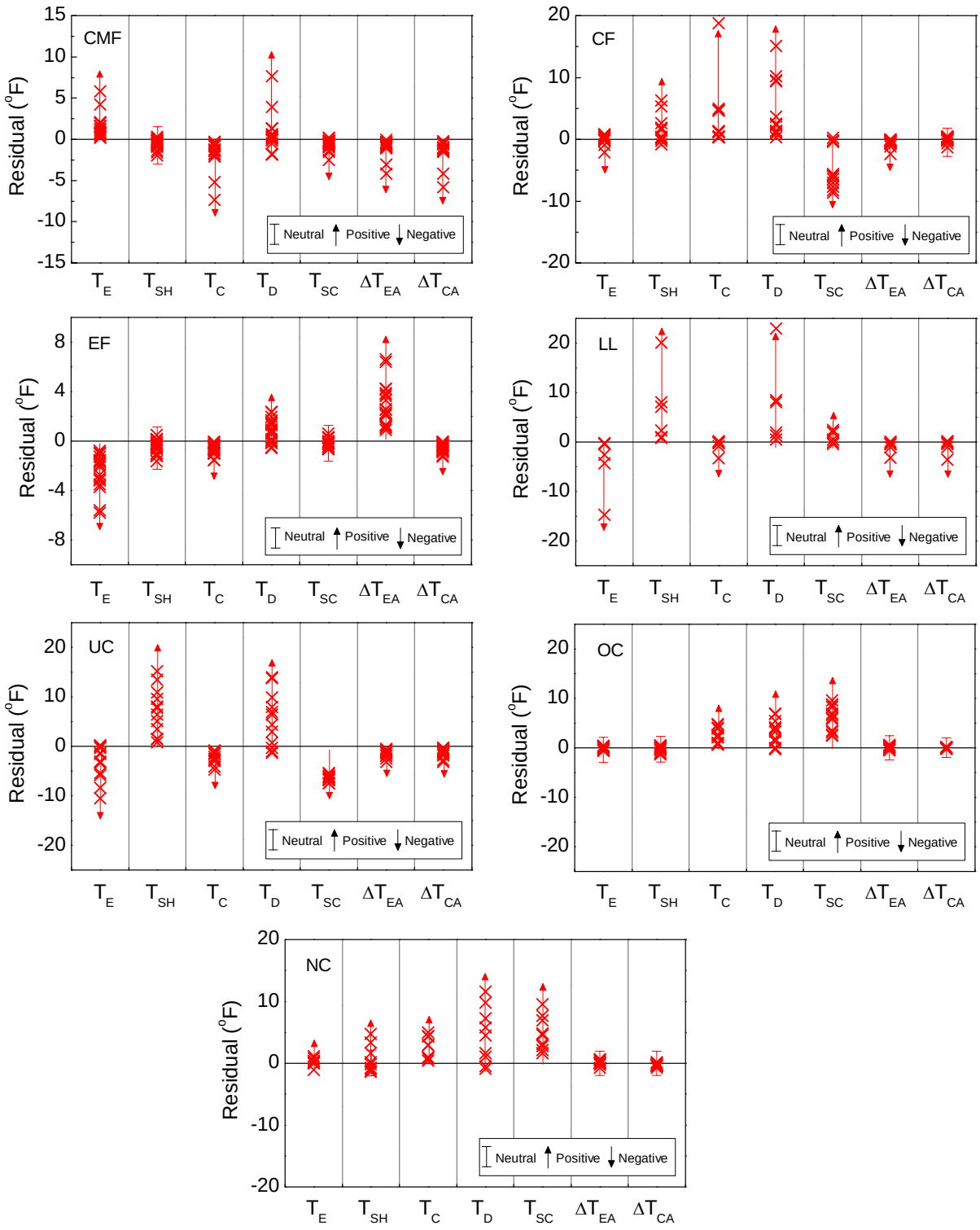

Figure 5.3. Residual patterns for different faults

Table 5.2. Rule-based FDD chart for air-to-air, single-speed heat pump in the cooling mode

Fault type	T_E	T_{SH}	T_C	T_D	T_{SC}	ΔT_{EA}	ΔT_{CA}
FF (Fault-free)	–	–	–	–	–	–	–
CMF (Compressor valve leakage)	↑	–	↓	↑	↓	↓	↓
CF (Improper outdoor air flow)	↓	↑	↑	↑	↓	↓	–
EF (Improper indoor air flow)	↓	–	↓	↑	–	↑	↓
LL (Liquid-line restriction)	↓	↑	↓	↑	↑	↓	↓
UC (Refrigerant undercharge)	↓	↑	↓	↑	↓	↓	↓
OC (Refrigerant overcharge)	–	–	↑	↑	↑	–	–
NC (Presence of non-condensable gases)	↑	↑	↑	↑	↑	–	–

The value of s must be determined so that it produces a given level of confidence that the currently measured value is within the neutral threshold (or outside this threshold). The confidence level is selected by the investigator; typical values of α are 0.01, 0.05, and 0.10, with corresponding confidence levels of $(1 - \alpha)$ of 0.99, 0.95, and 0.90 (Graybill and Iyer, 1994). In applying the s values, the user is determining the alarm thresholds for calling a fault or no-fault.

Table 5.3 shows standard deviations and thresholds with different zone densities for MPR(3rd order) models regressed to FDD test data. In general, if thresholds increase, the false alarm rate (FAR) decreases but missed detections increase, and vice versa. In this study, the threshold for a 95 % confidence level was applied to the FDD test data. Table 5.4 summarizes the standard deviations and thresholds for different domain coverage rates. Models with the best fit were

selected with respect to the domain coverage rate; the standard deviation and threshold prominently increased with a decrease of DCR.

Table 5.3. Standard deviation (^{o}F) of the fault-free model for different ZD (DCR=73 %, all data)

ZD	Applied model	$\sigma(T_E)$	$\sigma(T_{SH})$	$\sigma(T_C)$	$\sigma(T_D)$	$\sigma(T_{SC})$	$\sigma(\Delta T_{EA})$	$\sigma(\Delta T_{CA})$
All	3rd order MPR	0.124	0.314	0.077	0.310	0.191	0.124	0.112
100	3rd order MPR	0.133	0.322	0.081	0.318	0.195	0.135	0.114
50	3rd order MPR	0.147	0.388	0.093	0.521	0.219	0.156	0.117
25	3rd order MPR	0.149	0.420	0.094	0.590	0.236	0.159	0.119
10	3rd order MPR	0.144	0.432	0.093	0.597	0.258	0.157	0.121
5	3rd order MPR	0.141	0.433	0.097	0.589	0.258	0.158	0.125
1	3rd order MPR	0.144	0.442	0.099	0.537	0.277	0.166	0.138
$\varepsilon_{90\%}$	$1.65\cdot\sigma_{i.FF\ model}$							
$\varepsilon_{95\%}$	$1.96\cdot\sigma_{i.FF\ model}$							
$\varepsilon_{99\%}$	$2.58\cdot\sigma_{i.FF\ model}$							

Table 5.4. Standard deviation (^{o}F) of fault-free model for different DCR (ZD =100)

DCR (%)	Applied model	$\sigma(T_E)$	$\sigma(T_{SH})$	$\sigma(T_C)$	$\sigma(T_D)$	$\sigma(T_{SC})$	$\sigma(\Delta T_{EA})$	$\sigma(\Delta T_{CA})$
73	3rd order MPR	0.133	0.322	0.081	0.318	0.195	0.135	0.114
60	3rd order MPR	0.197	0.385	0.090	0.811	0.282	0.160	0.123
40	2nd order MPR	0.390	0.641	0.109	0.625	0.401	0.294	0.155
20	1st order MPR	0.673	0.659	0.196	2.111	0.393	0.523	0.196
$\varepsilon_{90\%}$	$1.65\cdot\sigma_{i.FF\ model}$							
$\varepsilon_{95\%}$	$1.96\cdot\sigma_{i.FF\ model}$							
$\varepsilon_{99\%}$	$2.58\cdot\sigma_{i.FF\ model}$							

5.3. Procedure for Testing and Rating FDD Performance

The faults summarized in Table 5.1 were part of the experimental dataset (Kim et al., 2006) applied to test FDD performance. For each dataset, the fault probability for eight conditions (FF, CMF, CF, EF, LL, UC, OC, and NC) was calculated using Equation 5.1 and the rule-based chart fault patterns as given in Table 5.2. Among the probabilities of the eight conditions, the fault type with the highest fault probability was selected as the fault type most likely occurring at the time. When the diagnosed fault type was the same as the originally imposed fault type, the diagnostic was considered successful. The goodness of the FDD method was further explored by applying the concepts of FDD performance evaluation as defined by Braun et al., (2012).

- Successful diagnosis rate, SDR (%): A fault is present. The summation of the detected and successfully diagnosed cases divided by total number of faulty tests equals the SDR for the particular fault.
- False alarm rate, FAR (%): No fault is present, but the protocol indicates the presence of a fault. The FAR equals the number of false alarm cases divided by the total number of fault-free tests.
- Missed detection rate, MDR (%): A fault is present, but the protocol indicates that no fault is present. The MDR equals the number of missed detection cases divided by the total number of faulty tests.
- Misdiagnosis rate, MSR (%): A fault is present. The protocol detects the fault but misdiagnoses the fault type. The MSR equals the number of misdiagnosis cases divided by the total number of fault-free and faulty tests.

The above performance indices address that the detection aspect of FDD (FAR and MDR) and the diagnosis (SDR and MSR).

As recommended in Section 4.3, the third order MPR model was applied for the fault-free model training. A zone coverage rate of 73 % represented all of the data and was used for this analysis. Figure 5.4 shows the SDR for the eight conditions with different zone densities. In the cases of FF, CMF, EF, and OC, the successful diagnosis rate (SDR, %) was relatively high; more than 80 % for all zone densities. The SDR of CF and UC was between 60 and 80 %, and that of LL and NC was less than 50 %. The feature pattern of the NC fault was very similar to that of OC, which was the reason for the inconsistent FDD performance on this fault (Figure 5.2). In the case of the LL fault, the fault pattern was unclear, and additional fault data for LL was needed since only six datasets were available for this fault case. Overall, the SDR gradually decreased when zone density was less than 100 or 50 due to the increase in the standard deviation of the fault-free models and neutral threshold width for a 95 % confidence (Figure 4.6). The average

SDR with a zone density of ALL and 100 was 83 % and 82 %, respectively, and gradually decreased from 75 % to 71 % as the zone density decreased.

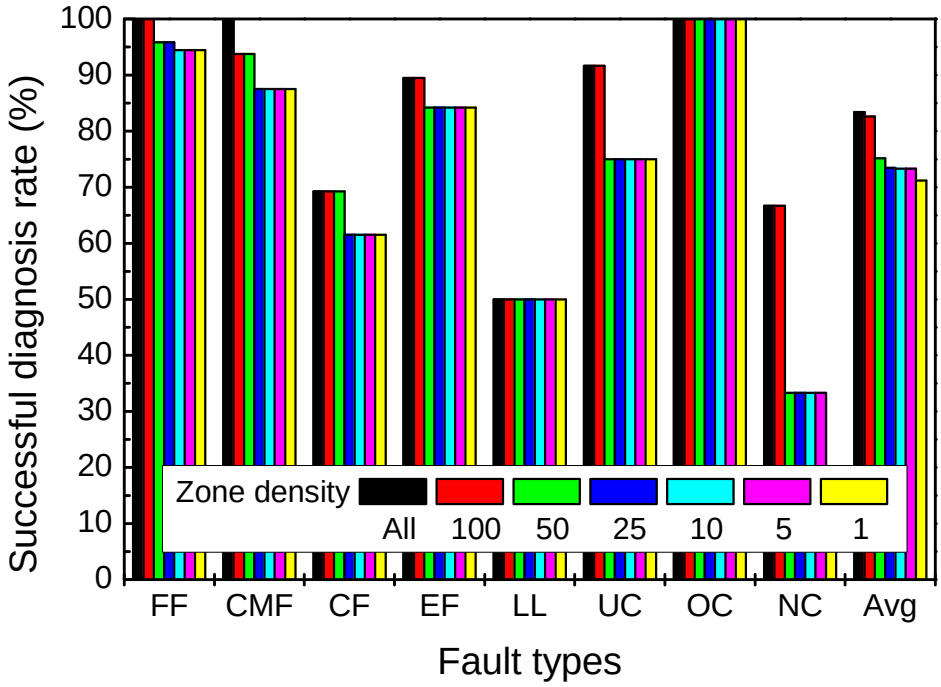

Figure 5.4. Successful diagnosis rate of various faults for different zone densities

False alarm, missed detection, misdiagnosis were analyzed with decreasing zone density, and presented in Figure 5.5. False alarm and missed detection were not observed at the tests with zone densities of ALL and 100. For zone densities less than 50 %, the false alarm case increased from 4.2 % to 5.6 % with decreasing zone density. Missed detections also increased from 3.6 % to 9.5 % with decreasing zone density. The FAR was less than 6 % and the MDR was less than 10 % at all zone density conditions. A zone density greater than 100 would be the best choice for a high quality FDD application due to the observed stability and predictive accuracy seen in our experimental dataset. Fault diagnosis performance with zone densities of ALL and 100 was also superior to cases with zone density less than 100. Misdiagnoses were 7.7 % and 8.3 % at zone densities of ALL and 100, respectively, with misdiagnoses distributed from 13.5 % to 16.2 % at zone densities less than 100.

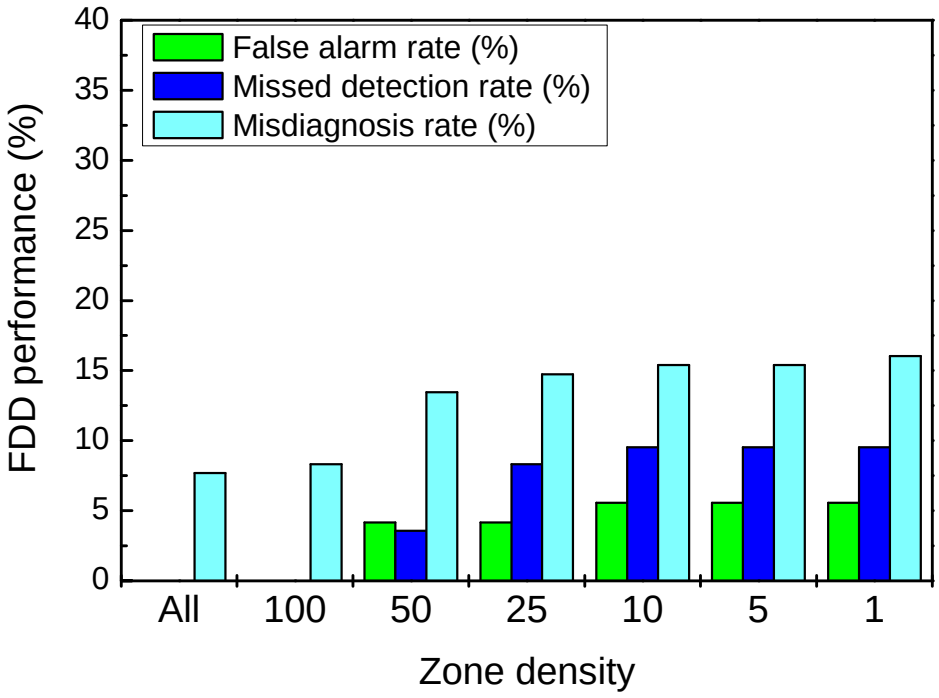

Figure 5.5. Fault detection and diagnostic performance for all eight conditions for different zone densities

5.4. Effect of Domain Coverage Rate on FDD Performance

As recommended in Section 4.4, the first order and second MPR models were applied for the fault-free models at a DCR of 20 % and from 40 % to 60 %, respectively. When the DCR was more than 60 %, the MPR(3rd order) model was applied to the fault-free model training. A zone density of 100 was applied for this analysis.

The successful diagnosis rate, SDR, for eight fault conditions and varying domain coverage rates are presented in Figure 5.6. With a DCR of 73 % and 60 %, the FF, CMF, EF, UC and OC faults showed an SDR of more than 85 %. The SDR of CF and NC faults was between 60 % and 70 %, and that of LL was less than 50 %. Exact diagnosis of FF is very important because it determines the fault detection performance (false alarm rate, FAR). In case of FF operation, the SDR drastically decreased below 65 % when the DCR was 20 %. In cases of CMF, EF, UC, and NC faults, the SDR significantly decreased at a DCR of 40 % and 20 % due to the increase in the standard deviation of the FF model and corresponding increase in the neutral threshold. The overall average SDR gradually decreased from 89 % to 61 % with the decrease of DCR from 73 % to 20 %.

Figure 5.7 shows FAR (false alarm rate), MDR (missed detection rate), and MSR (misdiagnosis rate) with the decrease of the DCR (domain coverage rate). False alarm and missed detection were not observed in the tests with zone coverage rate of 73 %. FAR was 1.39 % and 8.3 % at

DCR 60 % and 40 %, respectively, and then drastically increased to 37.5 % at DCR 20 %. MDR gradually increased from 7.14 % to 26.2 % with the decrease of DCR from 60 % to 20 %. MSR remained below 10 % at DCR 73 % and 60 %, and then the misdiagnosis rate steeply increased to 18.6 % and 38.5 % at a DCR of 40 % and 20 %. At a DCR from 73 % to 60 %, FAR, MDR, and MSR were all below 10 %. However, FDD performances worsened at DCRs from 40 % to 20 %. From Figures 5.6 and 5.7, DCRs greater than 60 % were recommendable for a high quality FDD application due stability and prediction accuracy. In addition, DCRs greater than 40 % might be acceptable for a lower quality FDD application if the fault detection error less than 15 % was allowable.

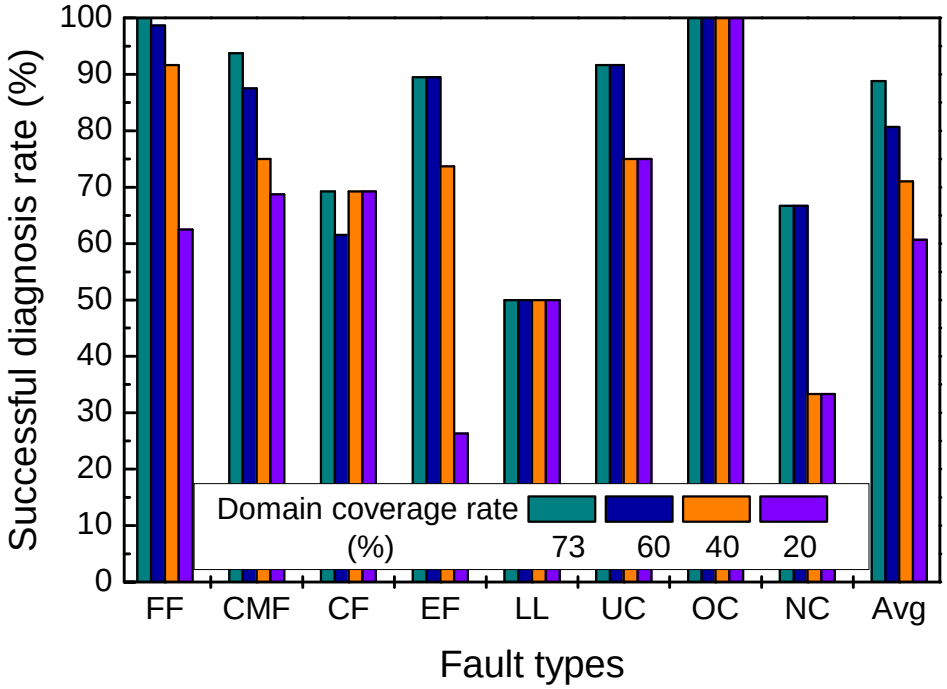

Figure 5.6. Successful diagnosis rate of various faults for different domain coverage rates

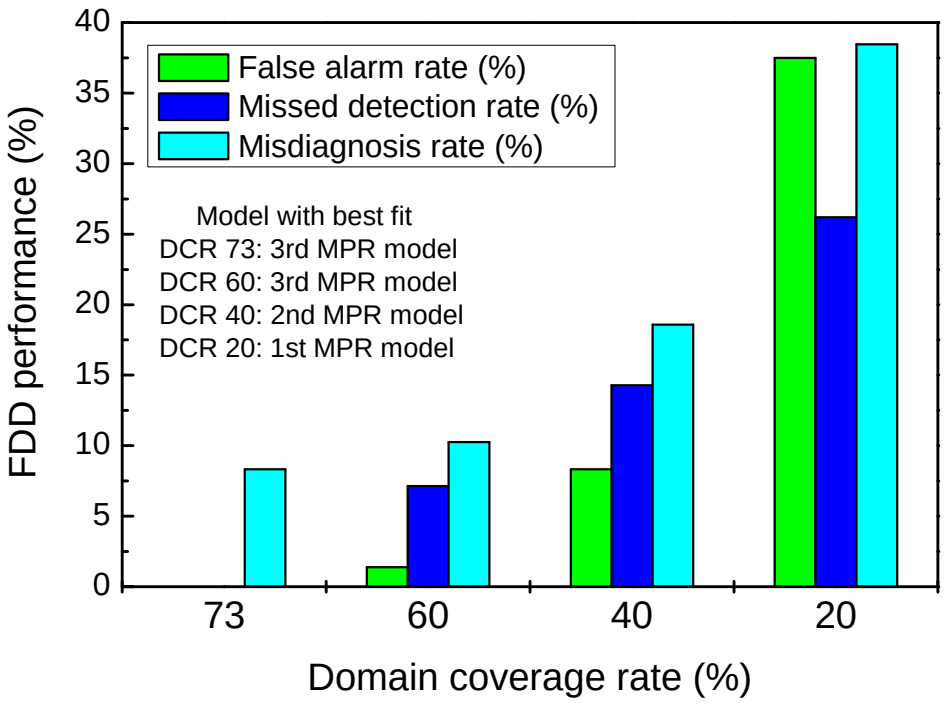

Figure 5.7. Fault detection and diagnostic performance for all faults for different domain coverage rates

6. Concluding Remarks

A concept for a self training, fault-free model for residential air conditioner fault detection and diagnosis was introduced and tested. The method of selecting the appropriate temperature domain for the fault-free system data was illustrated in order to cover most operating conditions considering different climate zones in the U.S. The fault-free system performance was modeled based upon three independent features (T_{OD}, T_{ID}, T_{IDP}) and seven dependent features (T_E, T_{SH}, T_C, T_D, T_{SC}, ΔT_{EA}, ΔT_{CA}). The new concept of zone density was introduced to manage and filter the system data. In addition, the new concept of domain coverage rate was also introduced to quantify the number of data needed to produce fault-free feature models.

Various fault-free models, such as the ANN (artificial neural network), the MPR (multivariable polynomial regression), and a combined ANN/MPR, were explored for implementing self training. The MPR method was shown to produce very good prediction performance (low standard errors) compared to the methods using ANNs. Therefore, MPR models were applied and tested against previously taken system data for additional analysis of self training.

For validation of the self training method, the full experimental dataset (72 fault-free and 84 fault tests) covering eight fault/conditions (fault-free, compressor valve leakage, outdoor coil air flow blockage, improper indoor air flow, liquid-line restriction, refrigerant undercharge,

refrigerant overcharge, and non-condensable gas contamination) was used to explore self training performance. The statistical rule-based fault classification method was illustrated.

FDD performance was analyzed using the successful detection rate (SDR), false alarm rate (FAR), missed detection rate (MDR), and misdiagnosis rate (MSR) as zone density (ZD) and domain coverage rate (DCR) were varied. This effort showed that a zone density greater than 100 was very successful within the experimental dataset. In addition, a domain coverage rate greater than 60 % produced acceptable FDD performance and good prediction performance (low standard errors).

This report attempts to document a mathematical and logical technique by which an FDD technique may be adapted to an air conditioning system with variations in installation details as would be seen in actual residences. It is by no means a perfected technique applicable to immediate deployment; many issues remain that still must be resolved by laboratory investigation and application to real world problems. When considering using an adaptive technique for FDD in a real application the following questions must be resolved:

1) What operating states are suitable for learning? Steady state is important, but what about heat pumps operating in frosting conditions for heating? What about the effects of rain on the outdoor unit? What about cooling operation at low outdoor temperatures when the TXV is operating at the edges of its steady control band? A key part of the learning algorithm is developing a filtering algorithm which picks only the data known to be good.

2) How does the FDD technique deal with the fact that the unit is aging and changing over time? In a real learning algorithm you must wait for the driving conditions to present themselves. If you install an air-conditioner in the Fall season, it could be 10 months before you see data for the hottest day. Is it fair to assume that the unit is unchanged since its install? What if the home owner/ tenant keeps their cooling setpoint at 75 °F all of the time? Now a new owner/tenant moves in and runs the house at 70 °F; can you use the old FDD model?

3) How do you deal with/quantify the noise seen in sensors installed in the field? Large transients and noise may be seen in sensor readings. A method of quantifying the sensor noises and creating dynamic error bands need to be developed. How does the FDD deal with a broken/malfunctioning sensor?

The next step is to take this idea to the laboratory and the field and start solving the outstanding issues.

References

AHRI. (2008). Performance rating of unitary airconditioning and airsource heat pump equipment, AHRI Standard 210/240. Arlington, VA, USA: Air-Conditioning, Heating, and Refrigeration Institute.

Baechler, M., Williamson, J., Gilbride, T., Cole, P., Hefty, M., Love, P. (2010). High-performance home technologies: Guide to determining climate regions by county. U.S. Department of Energy PNNL-19004.

Braun, J. (1999). Automated fault detection and diagnostics for vapor compression cooling equipment. International Journal of Heating, Ventilating, Air-Conditioning and Refrigerating Research, 5(2), 85-86.

Braun, J., & Li, H. (2001). Description of FDD modeling approach for normal performance expectation. West Lafayette, IN: Herrick Labs, Purdue University.

Braun, J., Yuill, D., Cheung, H. (2012). A method for evaluating diagnostic protocols for packaged air conditioning equipment CEC-500-08-049. West Lafayette, IN, USA: Purdue University Herrick Laboratories.

Chen, B., Braun, J. E. (2001). Simple rule-based methods for fault detection and diagnostics applied to packaged air conditioners. ASHRAE Transactions, 107(1), 847-857.

Cho, J., Heo, J., Payne, W., Domanski, P. (2014). Normalized performances for a residential heat pump in the cooling mode with single faults imposed. Applied Thermal Engineering, 67, 1-15.

EIA 2013, U.S. Energy Information Agency, Residential Energy Consumption Survey, http://www.eia.gov/electricity/sales_revenue_price/pdf/table5_a.pdf (Accessed April 2015).

EIA 2014, U.S. Energy Information Agency, Residential Energy Consumption Survey, http://www.eia.gov/tools/faqs/faq.cfm?id=96&t=3 (Accessed April 2015).

Frenz, C. (2002). Visual basic and visual basic.net for scientists and engineers. Apress. 1st Edition. February.

Graybill, F., Iyer, H. (1994). Regression analysis: Concepts and applications second ed. Belmont, CA, USA: Duxbury Press.

Heo, J., Payne, W., Domanski, P. (2012). FDD CX: A fault detection and diagnostic commissioning tool for residential air conditioners and heat pump, NIST TN 1774. Gaithersburg, MD: National Institute of Standards and Technology.

Kim, M., Payne, W., Domanski, P., Hermes, C. (2006). Performance of a Residential Air Conditioner at Single-Fault and Multiple-Fault Conditions, NISTIR 7350. Gaithersburg, MD: National Institute of Standards and Technology.

Kim, M., Yoon, S., Domanski, P., Payne, W. (2008a). Design of a steady-state detector for fault detection and diagnosis of a residential air conditioner. Int. J. Refrig. 31, 790-799.

Kim, M., Yoon, S., Payne, W., Domanski, P. (2008b). Cooling mode fault detection and diagnosis method for a residential heat pump, NIST SP 1087. Gaithersburg, MD: National Institute of Standards and Technology.

Kim, M., Yoon, S., Payne, W., Domanski, P. (2010). Development of the reference model for a residential heat pump system for cooling mode fault detection and diagnosis. Journal of Mechanical Science and Technology, 24(7), 1481-1489.

Li, H., Braun, J. (2003). An improved method for fault detection and diagnosis applied to packaged air conditioners. ASHRAE Transactions, 109(2), 683-692.

Payne, W., Domanski, P., Yoon, S. (2009). Heating mode performance measurements for a residential heat pump with single-faults imposed, NIST TN 1648. Gaithersburg, MD: National Institute of Standards and Technology.

Rossi, T., Braun, J. E. (1997). A statistical rule-based fault detection and diagnostic method for vapor compression air conditioners. HVAC&R Research, 3(1), 19-37.

Thornton, B., Wang, W., Lane, M., Rosenberg, M., Liu, B. (2009). Technical support document: 50 % energy savings design technology packages for medium office buildings. U.S. Department of Energy, PNNL-19004.

Yoon, S., Payne, W., Domanski, P. (2011). Residential heat pump heating performance with single faults imposed. Applied Thermal Engineering, 31, 765-771.

Acknowledgements

The authors would like to acknowledge Min Sung Kim (Chief, Thermal Energy Conversion Laboratory, Korea Institute of Energy Research – KIER), Seok Ho Yoon (Korea Institute of Machinery and Materials), Jin Min Cho, and Young-Jin Baik (Engineer, Thermal Energy Conversion Laboratory, Korea Institute of Energy Research – KIER) for their work in developing the background material used in this report. Also, John Wamsley, Glen Glaeser, and Art Ellison provided technician support for collecting the data used to develop FDD fault-free feature correlations. We also would like to thank Will Guthrie of the NIST Statistical Engineering Division for reviewing the statistical FDD method section and Dan Veronica of the NIST Energy and Environment Division for reviewing and commenting on the entire document.

Appendix A. Temperature Data Distribution

The temperature domain should be selected in order to cover most of the operating conditions a residential air conditioner may experience. As summarized in Appendix A and Table A.1, the U.S. climate may be divided into seven climate zones based upon certain criteria (Baechler et al., 2010). Seven representative cities within these zones were chosen as a source for temperature and humidity data (Thornton et al., 2009). The most recent five year climate data were investigated as shown in Figure A.2. Temperature data domains for outdoor and indoor temperature with relative humidity were determined using data for these seven cities.

Table A.1. Temperature domain by climate zone

Temp. domain	Hot humid	Hot dry	Mixed humid	Mixed dry	Marine	Cold	Very cold
T_{OD}	80 to 105 by a step of 5 °F (5 zones)	80 to 100 by a step of 5 °F (4 zones)	80 to 105 by a step of 5 °F (5 zones)	80 to 105 by a step of 5 °F (5 zones)	80 to 95 by a step of 5 °F (3 zones)	80 to 100 by a step of 5 °F (4 zones)	80 to 95 by a step of 5 °F (3 zones)
T_{ID}	65 to 85 by a step of 5 °F (4 zones)						
RH	20 to 80 by a step of 20 % (3 zones)						

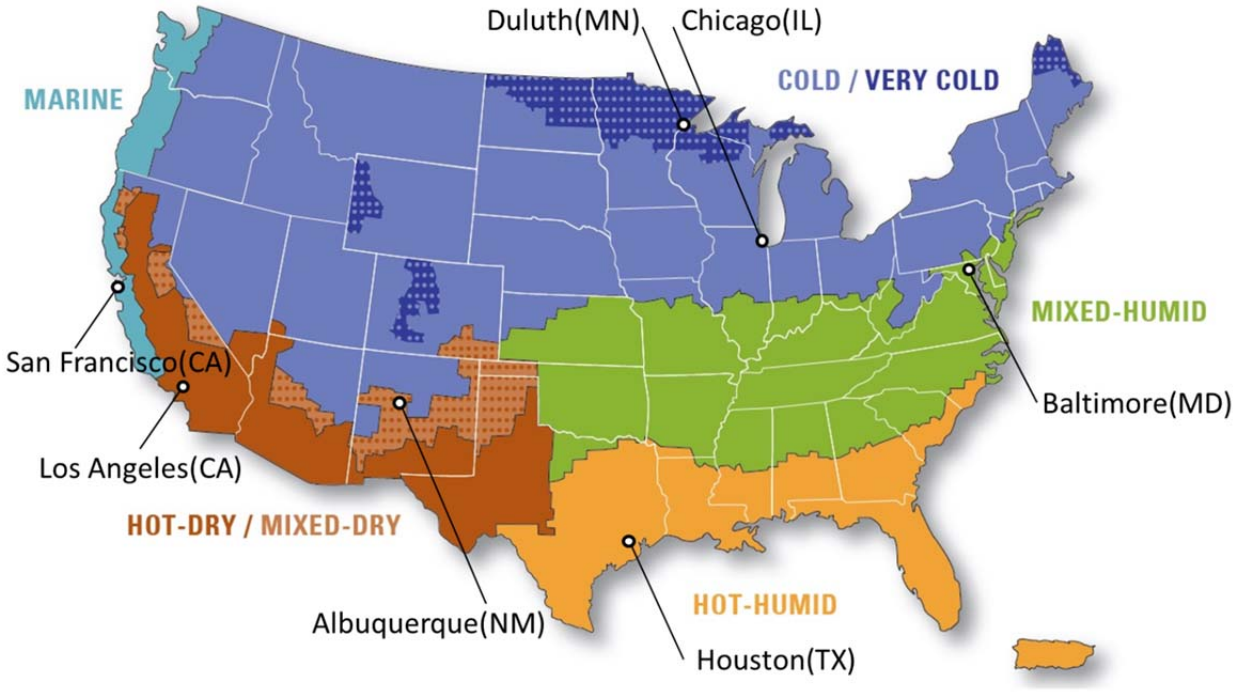

Figure A.1 Representative cities for seven US climate zones

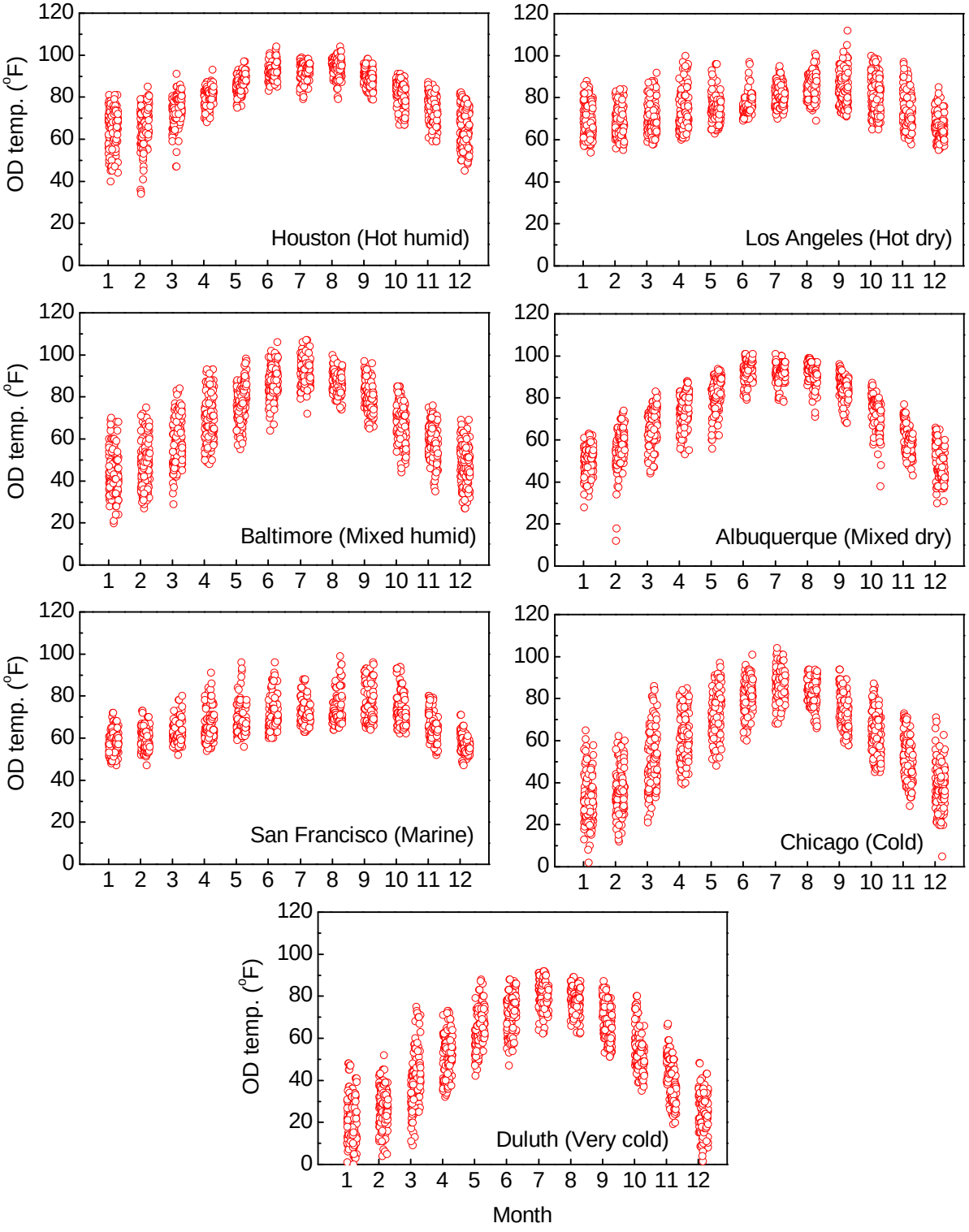

Figure A.2 Maximum outdoor temperature distributions in seven climate zones from 2008 to 2012